



## **DETECTION AND DELINEATION OF GEOTHERMAL RESOURCES USING 1D JOINT INVERSION OF MT AND TEM DATA WITH PRACTICAL APPLICATIONS FROM REYKJANES GEOTHERMAL FIELD, SW-ICELAND**

**Ronald Togo Verave**

Mineral Resources Authority  
Geological Survey Division  
Mining Haus, Poreporena Freeway  
P.O. Box 1906, Port Moresby, 121  
PAPUA NEW GUINEA  
*rverave@mra.gov.pg*

### **ABSTRACT**

Geophysical exploration is a vital part of geothermal prospecting, particularly during the initial stages of development. When conducted alongside geological and geochemical work, a better understanding of the subsurface of the geothermal resource and its characteristics can be obtained. The resistivity methods in geophysical exploration are considered the most powerful geophysical tool in prospecting for high-temperature geothermal resources. This is because the subsurface distribution of resistivity can tell about the parameters that directly influence the geothermal system. A typical alteration distribution in a high-temperature geothermal field is expected but it is subject to the elevation of the area and its distance to the coast. Systems close to the coast do not tend to have as sharp a correlation between alteration and subsurface resistivity (e.g. Reykjanes, SW-Iceland) as systems further away from the coast; this is due to the high salinity in the geothermal fluids. 1D joint inversion of TEM and MT data was done to remove the static shift of the MT data from the Reykjanes geothermal field. Results from the 1D joint inversion revealed a homogeneous low resistivity at shallow depths as was discovered by past studies in the area. An iso-resistivity map at a depth of 10,000 m revealed two heat sources, one to the southwest and another to the northeast. They are associated with deep seated intersecting fractures and faults.

### **1. INTRODUCTION**

The global geothermal energy outlook is gaining momentum as it is becoming more feasible to develop today than it used to be in the past. An increase in knowledge and technology in exploration, drilling and reservoir engineering has resulted in advancements in geothermal electrical generation and exploration. The advancements were driven by technologies used in oil and gas prospecting and also from mining.

Geothermal energy is the heat energy produced in the core of the earth that can be harnessed to generate electrical energy or for a wide range of direct uses such as district heating, bathing etc.

The main objective in the early stages of geothermal energy development is detecting and defining the extent of a geothermal resource, siting wells and understanding the characteristics of the geothermal reservoir. This information is usually obtained during the initial stages of geothermal development where geophysical exploration, geological surface exploration and geochemical exploration are carried out.

Geophysical exploration plays an important role in achieving these objectives. Resistivity methods and thermal methods are proven to be the most powerful geothermal tools in geothermal prospecting because they detect parameters that are directly influenced by geothermal activity.

This report focuses mainly on two resistivity methods, Transient Electromagnetics (TEM) and Magnetotellurics (MT). TEM and MT are the two resistivity methods most intensely used for geothermal prospecting in the world. It discusses the process involved in 1D joint inversion of TEM and MT data, their results and interpretations using examples from the Reykjanes high-temperature geothermal field, SW-Iceland. TEM and MT field procedures and data acquisition are also discussed with some fundamental concepts presented in the background section of this report.

## 2. BACKGROUND

### 2.1 Resistivity and geothermal systems

In high-temperature geothermal systems, subsurface resistivity is used to describe the relationship between the parameters that characterize the geothermal system and its history. It is one of the most valuable physical properties of materials and has proven to be the most useful geophysical parameter in the search for geothermal resources (Ussher et al., 2000). Therefore, it is paramount to gain a better understanding of the resistivity of rocks and the parameters that correlate to the geothermal activity (Georgsson, 2013).

#### 2.1.1 What is resistivity?

Specific resistivity,  $\rho$ , is defined through Ohm's law. The electrical field strength,  $\vec{E}$  [V/m] at a point in a material is proportional to the current density,  $\vec{j}$  [A/m<sup>2</sup>]:

$$\vec{E} = \rho \vec{j} \quad (1)$$

The proportionality constant,  $\rho$ , depends on the material and is called the specific resistivity, measured in  $\Omega\text{m}$ . The reciprocal of resistivity is conductivity ( $1/\rho = \sigma$ ).

Resistivity can also be defined as the ratio of the potential difference,  $\Delta V$  [V/m], to the current,  $I$  [A], across a material which has a cross-sectional area of 1 m<sup>2</sup> and is 1 m long.

$$\rho = E/j = \Delta V/L \cdot S/I \text{ and since } E = \Delta V/L \text{ and } j = I/S \text{ then } \rho = \Delta V/I \quad (2)$$

#### 2.1.2 Electrical resistivity of water bearing rocks

The conductivity of most rocks reflects the electrolytic conduction by the aqueous solution of common salts present in the pores of rocks and conduction at the rock-water boundary. The resistivity is controlled by parameters listed below:

- *Porosity and pore structure of the rock*  
Porosity is basically the ratio of the pore volume and the total volume of a material. There are three main types:

- intergranular, where the pores are formed as spaces between grains or particles in compact materials like sediments and volcanic ash
- joints-fissures or fractures, where the pores are formed by a net of fine fissures caused by tectonics or cooling of the rocks (igneous rocks, lava)
- vugular porosity, where big and irregular pores have been formed due to the dissolution of material evident in limestone formations.

In order for conduction to occur through the pores, the pores must be interconnected and water filled or saturated. Water saturated pores conduct electricity along the connected pores and the relationship is that the pores in a formation are resistive if the voids are free from water. The reverse happens when the pores are filled and are interconnected.

- *Conductivity of the rock matrix*

In geothermal conditions, the rock matrix itself acts as an insulator at reservoir temperatures and has poor conductivity. The only way conduction is possible is through the presence of fluid and ions in rocks and by electrons in minerals at the rock-water interface. This is contrary to conditions of very high temperature where rocks first start to melt. Here we see the matrix conductivity follows the Arrhenius formula:

$$\sigma_m(T) = \sigma_0 e^{-E/kT} \quad (3)$$

Flóvenz et al. (2012) showed, based on work done by Scarlato et al. (2004), that basalts and related materials over the temperature range of 400-900°C give values of 0.80 for E and 300 for  $\sigma_m$ , which means that the matrix resistivity of basaltic rocks is in the order of 1000  $\Omega\text{m}$  at 400°C and decreases to 10  $\Omega\text{m}$  at 800°C.

Partial melt will still increase conductivity at high temperatures. For instance, in the roots of geothermal systems where temperatures exceed 400°C, the matrix conductivity is basically responsible for the overall conductivity.

- *Water rock interaction and the mineral assemblage, alteration*

In high-temperature geothermal systems, water-rock interaction produces alteration (secondary) minerals. The type of minerals formed depends upon the chemical composition of the host-rocks, pore fluid and temperature.

The amount of alteration depends upon time, permeability and the chemical composition and texture of the rocks. The alteration minerals lining the walls of the fractures seem to control, to a large extent, the electrical resistivity in rocks up to temperatures of 200-250°C.

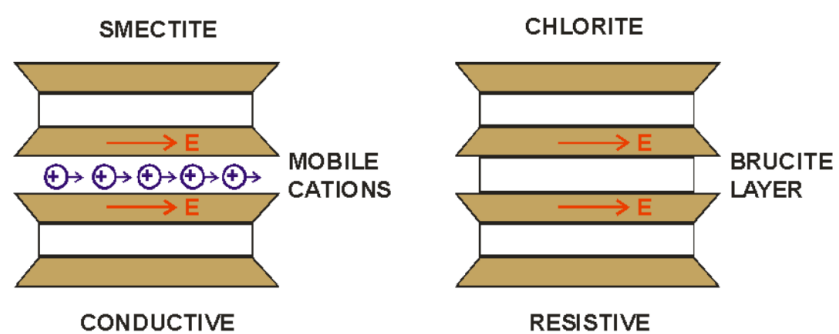


FIGURE 1: Smectite and chlorite mobile cations distributions (Hersir, 2013)

Some of the alteration minerals are conductive while others are less conductive or resistive (see Figure 1). Smectite/zeolites have loosely bound cations that make them conductive. In chlorite, the ions are bound in a crystal lattice, making them resistive.

- CEC (cation-exchange capacity) for smectite is: 0.8-1.5 meq/g
- CEC for chlorite is: 0.01 meq/g

- *Temperature*

The relationship between temperature and the resistivity of an aqueous solution is described by Dakhnov (1962) through the equation below:

$$\rho_w = \frac{\rho_{wo}}{1 + \alpha(T - T_0)} \quad (4)$$

$\rho_{wo}$  ( $\Omega\text{m}$ ) is the resistivity of the fluid at temperature  $T_0$ ,  $\alpha$  is the temperature coefficient of resistivity, where the value of  $\alpha$  is approximated to  $0.023^\circ\text{C}^{-1}$  at  $T_0 = 25^\circ\text{C}$ .

It is generalised that, at temperatures of  $0\text{--}200^\circ\text{C}$ , resistivity of aqueous solutions decreases with increasing temperature. This is caused by increasing mobility of the ions caused by a decrease in the viscosity of the water. At high temperatures, a decrease in the dielectric permittivity of the water results in a decrease in the number of dissociated ions in the solution. This starts to increase fluid resistivity, usually above  $300^\circ\text{C}$  (Quist and Marshall, 1968), as shown in Figure 2 (at left).

- *The degree of fluid saturation*

Below the ground water table, the rocks in geothermal areas are generally saturated by water and steam. Thus, the groundwater table is the mark at which conductivity is prominent, thereby indicating significant water saturation. The layers above the groundwater table could be partially saturated and the resistivity there depends upon the degree of saturation in the rocks.

- *Salinity of pore fluid*

Salinity of fluids in high-temperature geothermal systems is expected and it affects resistivity measurements to some degree. There is a nearly linear relationship between salinity and resistivity as seen in Figure 2 (at right).

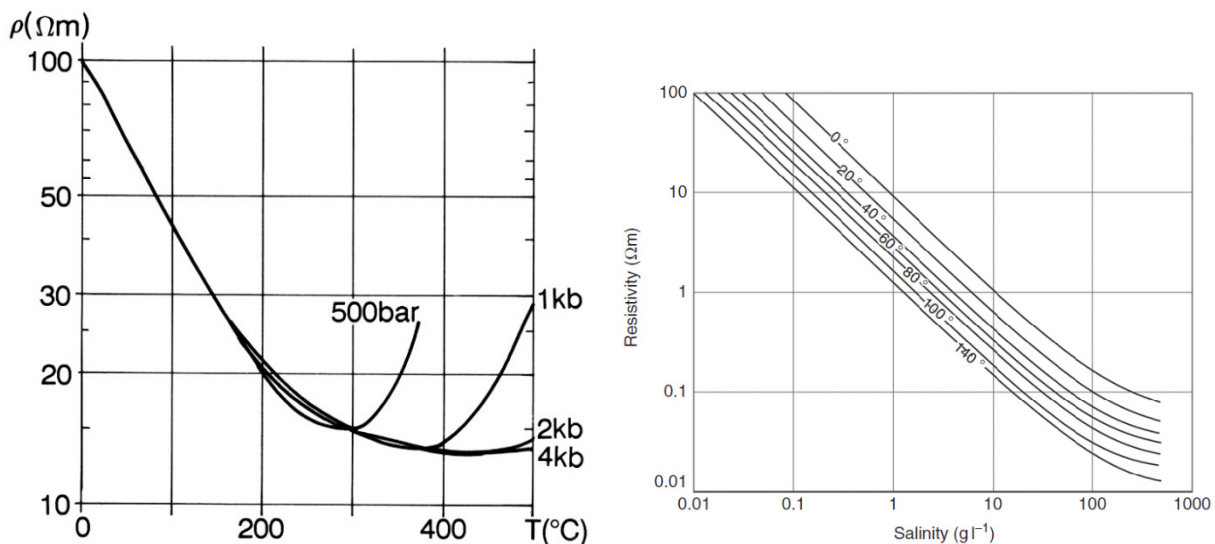


FIGURE 2: Left – electrical resistivity as a function of temperature at different pressures (Flóvenz et al., 2012; based on Quist and Marshall, 1968); Right – resistivity as a function of salinity (Flóvenz et al., 2012; based on Keller and Frischknecht, 1966)

These parameters are described in detail by Flóvenz et al. (2012) who generalised that at typical reservoir temperatures, the conduction in the rock matrix is normally negligible. The main contributors to the electrical conduction in geothermal reservoirs are conduction by dissolved ions in the pore fluid (pore-fluid conduction) and conduction by absorbed ions on the pore surface (interface or surface conduction).

Electrical conductivity in minerals and solutions takes place by the movement of electrons and ions. Most rocks near the earth's surface have low conductivity. Conduction of electricity is mostly through groundwater contained in rock pores and along surface layers at the contact of rocks and solution.

### 2.1.3 Association between high temperature and clay alteration

Hydrothermal alteration has successfully been used to define several parameters of geothermal systems such as the temperature distribution, permeability and thermal evolution. The association between temperature and clay alteration arrangements is well established and can be used as a tool for predicting temperature during drilling. Inferred correlations between alteration types and resistivity can extend this further to enable better prediction of reservoir temperature from surface geophysical measurements.

In a high-temperature geothermal field in volcanic areas, geothermal fluids are sometimes saline and hydrothermal alterations cause pervasive changes to the natural resistivity of rocks in which the system develops. Generally, the salinity and the clay alteration, combined with the high temperatures produced by the geothermal activity, tend to create a lower overall resistivity in geothermal systems.

Commonly noticed as we gradually progress from surface to deeper levels, is a high resistivity above the low-temperature zone; this is interpreted as a zone that may tend to have poor water-saturation, minimal hydrothermal alteration and little reduction of resistivity by temperature. This can be referred to as the cool upper part of the system where there is no alteration at temperature less than 70°C.

The highly conductive zone at intermediate temperatures is widely known as a characteristic of geothermal systems. Low resistivity in this zone is correlated with clay hydrothermal alteration predominantly made up of smectite/zeolite minerals (Árnason et al., 1987a). This low-resistivity zone in the past was often regarded as being associated with the hot saline fluids of the geothermal systems (Ussher et al., 2000). This may have been true for high-salinity reservoirs such as those in western USA. Temperatures of 70-230°C were encountered there with low resistivity of the order of 1-10  $\Omega\text{m}$ .

At still deeper levels, the higher resistivity found in the core of the system is correlated with some vapour-dominated reservoirs but is characteristic of most low-moderate salinity reservoirs. This layer is below the overlying conductive zone and the high resistivity is due to the rock matrix being less conductive than the saturated fluids, because low conductivity alteration products dominate mineralisation. Temperatures here are above 230°C, and typical resistivity values are greater than 10  $\Omega\text{m}$  (Ussher et al., 2000).

Figure 3 shows a resistivity cross-section taken from the Nesjavellir high-temperature geothermal field in SW-Iceland. It depicts the resistive structure of a high-temperature geothermal field in association with the alteration

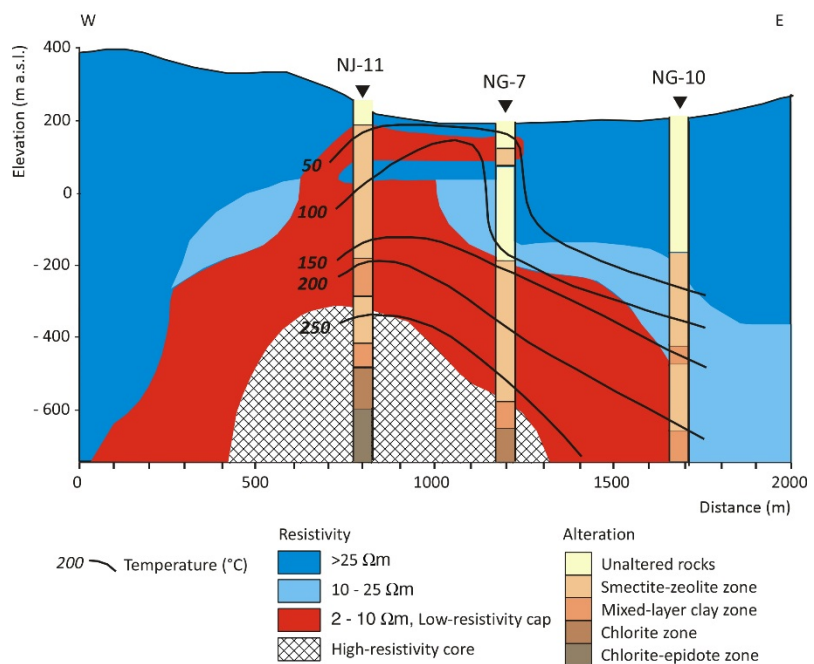


FIGURE 3. Typical resistivity structure of a high-temperature geothermal reservoir showing a high-resistivity core beneath a low-resistivity cap based on 2D interpretation of a detailed multi-method DC resistivity survey from 1985 and 1986 (Árnason et al., 1987b)

temperatures and minerals as described above. The up-doming low-resistivity cap is predominantly controlled by highly conductive alteration minerals, like smectite and zeolite which have a high cation exchange capacity (CEC). The alteration temperatures smectite/zeolite dominate the temperature interval between 100 and 230°C. The highly resistive core below is contained by the conductive cap where alteration minerals such as chlorite and epidote are dominant. The presence of these minerals makes these layers more resistive because the ions in chlorite and epidote are bound in crystal lattices, making them resistive. The low CEC of chlorite contributes immensely to the resistive nature of chlorite.

To tell whether the system is fossil or young cannot be answered by uncovering the subsurface resistivity distribution alone. Delineating resistivity anomalies in high-temperature geothermal fields reflects the subsurface alterations but not necessarily the temperature within the system. The alteration temperatures and the formation temperature have to be at equilibrium in order to infer temperatures through subsurface resistivity. In a younger geothermal system, the alteration temperature lags behind the formation temperature, while in a fossil geothermal system the alteration temperatures are higher than the formation temperature.

## **2.2 Geophysical exploration methods in geothermal prospecting**

Geophysical exploration of geothermal resources deals with the measurement of the physical properties of the earth. In geothermal exploration the resistive property of the earth and its thermal distribution are most useful entities which can describe parameters that are directly influenced by geothermal activity. Resistivity and thermal methods are, therefore, called the direct methods while other methods, referred to as indirect or structural methods, explore the physical parameters of the host rock, such as magnetic properties, density and seismic velocity.

In the following discussion, the emphasis is on the resistivity methods, particularly TEM and MT, and their application in geothermal exploration. Although it must be clear that it is important to combine different methods to obtain adequate information to give a better understanding of the geothermal system.

The idea behind all resistivity methods is to induce an electrical current into the earth and monitor signals, normally at the surface, generated by the current distribution. The three main resistivity electrical sounding methods are the DC sounding method, TEM and MT.

The DC Schlumberger method was extensively used in the 1970s and 1980s. In conventional direct current soundings, such as Schlumberger soundings, this is done by injecting current into the ground through electrodes at the surface; the signal measured is the electric field (the potential difference over a short distance) generated at the surface. In magnetotellurics (MT), the current in the ground is induced by time variations in the earth's magnetic field, and the signal measured is the electric field at the surface. In transient electromagnetics (TEM), the current is also induced by a time-varying magnetic field but, in this case, the current source is not the natural field; the source is of a controlled magnitude generated by current in a loop or a grounded dipole and the monitored signal is the decaying magnetic field at the surface.

### **2.2.1 Basic theory of TEM**

There exist several methods of TEM measurements, varying only by source type (loop source or dipole source) and the positioning of the receiver in relation to the source (Flóvenz et al., 2012). This record describes a configuration of the central-loop TEM setup where the receiver is placed in the middle of the source loop. TEM was introduced into the geothermal exploration realm in the 1980s with refinements done during the decade. The central loop TEM method was first tested for geothermal exploration in Iceland in the summer of 1986 (Árnason et al., 1987b).

TEM makes use of a magnetic field to induce currents in the earth. In the central loop TEM sounding method, a constant magnetic field is built up by transmitting strong current through a big loop (Figure 4). Then the current is abruptly turned off. The decaying magnetic field induces secondary currents and a secondary magnetic field, decaying with time. The decay rate of the secondary field is monitored by measuring the voltage induced in a receiver coil (or small loop) in the centre of the transmitting loop. Current distribution and the decay rate are recorded as a function of time dependent on the resistivity of structures in the earth, and can be interpreted in terms of the subsurface resistivity structure (Georgsson, 2013).

$\rho_a$  is a function of several variables. This includes measured voltage; time elapsed from turn off; area of loops/coils; number of windings in loops/coils; and magnetic permeability.

For a homogeneous half-space, the apparent resistivity  $\rho_a$ , is expressed in terms of induced voltages at late times (Figure 5) after the source current is turned off and is given by:

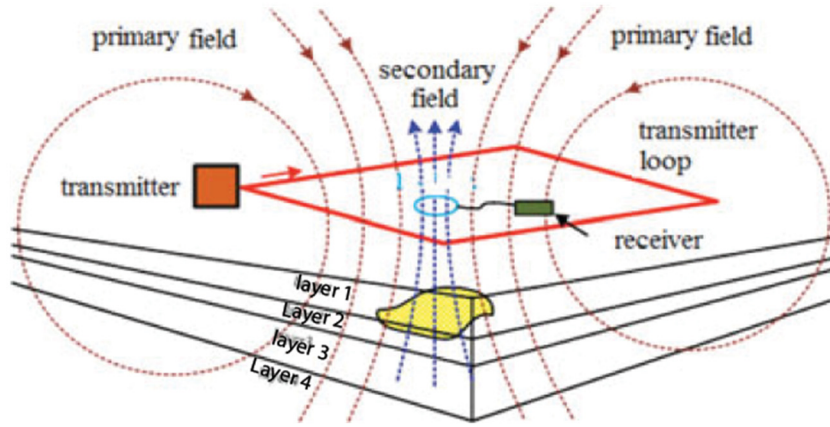


FIGURE 4: Layout of TEM field configuration (modified from Xue et al., 2013)

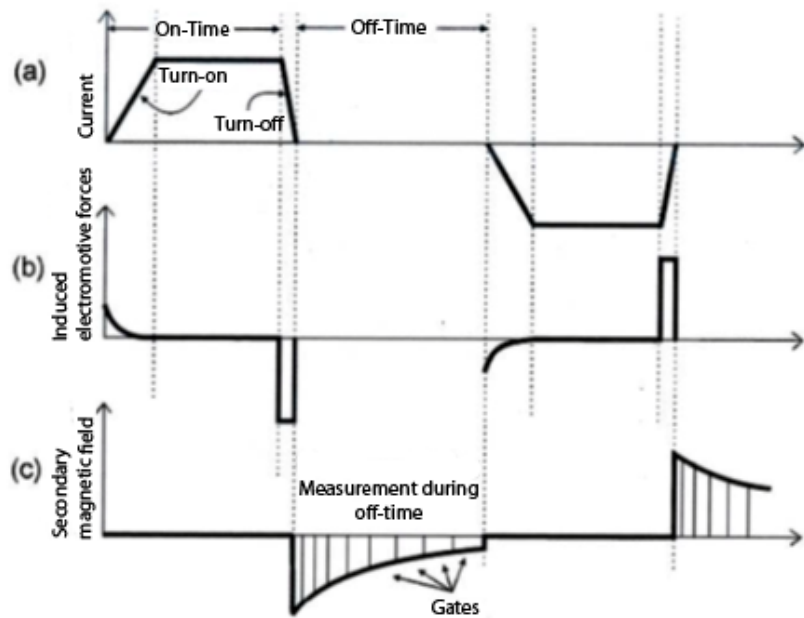


FIGURE 5: Time gates showing pattern during early time and late time responses (modified from Rowland, 2002)

$$\rho_a = \frac{\mu_0}{4\pi} \left[ \frac{2\mu_0 A_r n_r A_s n_s I_0}{5t^{5/2} V(t, r)} \right]^{2/3} \quad (5)$$

- where  $t$  = Time elapsed after the transmitter current is turned to zero (s);
- $V(t, r)$  = Measured voltage in the receiver loop (V);
- $A_r$  = Cross-sectional area of the receiver loop (m<sup>2</sup>);
- $n_r$  = Number of windings in the receiver loop;
- $A_s$  = Cross-sectional area of the transmitter loop (m<sup>2</sup>);
- $n_s$  = Number of windings in the transmitter loop;
- $\mu_0$  = Magnetic permeability in vacuum (H/m);
- $r$  = Radius of transmitter loop (m).

To see how Equation 5 is derived, the reader is referred to Árnason (1989).

### 2.2.2 Basic theory of MT

The magnetotelluric method or magnetotellurics (MT) is an electromagnetic geophysical exploration technique that images the electrical properties (distribution) of the earth at subsurface depths. The energy for the magnetotelluric technique is from natural sources of external origin. When this external energy, known as the primary electromagnetic field, reaches the earth's surface, part of it is reflected back and the remaining part penetrates the earth. Earth acts as a good conductor, thus, electric current (known as telluric currents) are induced, in turn producing a secondary magnetic field.

The MT method was first introduced by Tikhonov (1950) and Cagniard (1953) and further by Cantwell (1960) and Vozoff (1972, 1991). Measurements from the horizontal component of the natural electromagnetic field are used to construct the full complex impedance tensor,  $Z$ , as a function of the frequency. The relationships between the electrical and the magnetic field can be best described by assuming the following equation which was taken from (Hersir et al., 2013):

$$\begin{bmatrix} E_x \\ E_y \end{bmatrix} = \begin{bmatrix} Z_{xx} & Z_{xy} \\ Z_{yx} & Z_{yy} \end{bmatrix} \begin{bmatrix} H_x \\ H_y \end{bmatrix} \quad (6a)$$

or in matrix form:

$$\vec{E} = Z\vec{H} \quad (6b)$$

where  $\vec{E}$  and  $\vec{H}$  are the electrical and magnetic field vectors (in the frequency domain), respectively, and  $Z$  is a complex impedance tensor which contains information on the subsurface resistivity structure.

For a homogeneous and 1D earth,  $Z_{xy} = -Z_{yx}$  and  $Z_{xx} = Z_{yy} = 0$ . For a 2D earth, resistivity varies with depth and in one horizontal direction, it is possible to rotate the coordinate system such that  $Z_{xx} = Z_{yy} = 0$ , but  $Z_{xy} \neq Z_{yx}$ . For a 3D earth, all the impedance tensor elements are different.

From the impedances, the apparent resistivity ( $\rho$ ) and phases ( $\theta$ ) for each frequency can be calculated as:

$$\rho_{xy} = 0.2T|Z_{xy}|^2 = 0.2T \left| \frac{E_x}{H_y} \right|^2; \theta_{xy} = \text{arg}(Z_{xy}) \quad (7a)$$

$$\rho_{yx} = 0.2T|Z_{yx}|^2 = 0.2T \left| \frac{E_y}{H_x} \right|^2; \theta_{yx} = \text{arg}(Z_{yx}) \quad (7b)$$

How deep the MT soundings can probe is dependent on the wavelength of the recorded EM fields and the subsurface resistivity structure. The longer the period  $T$ , the deeper it penetrates and vice versa. Skin depth, sometimes referred to as the penetration depth ( $\delta$ ), describes the relationship between the varying magnitude of the period  $T$  and the depth of penetration and is given by:

$$\delta(T) \approx 500\sqrt{T\rho} \text{ (m)} \quad (8)$$

where the EM fields have attenuated to a value of  $e^{-1}$  (0.37) of their surface amplitude.  $\rho$  is the average resistivity of the subsurface down to that depth (Flóvenz et al., 2012).

Time series data acquired are transformed into the frequency domain, and auto- and cross-power spectra are calculated to estimate the impedance tensor as a function of frequency. The determinant of the impedance tensor, which is also called the effective impedance,  $Z_{DET}$  (Pedersen and Engels, 2005), is defined as:

$$Z_{DET} = \sqrt{Z_{xx}Z_{yy} - Z_{xy}Z_{yx}} \quad (9)$$

The effective impedance can be used to compute the determinant apparent resistivities and phase. For all current directions, a useful average of the impedance is best derived from the determinant data.

### 2.2.3 Static shifts

The presence of near surface resistivity inhomogeneities can distort the electrical field, since the field is not continuous across resistivity boundary. This galvanic distortion effect is known as static shift. This effect shifts the MT apparent resistivity sounding curve (i.e.,  $\log \rho_a$  vs.  $\log T$ ) by some constant scale factor. Static shift does not affect the phases of the MT impedance tensor. Since a magnetic field is relatively unaffected by surface inhomogeneities, controlled-source magnetic-field soundings such as Central-loop Transient Electromagnetic (TEM) soundings can be used to correct for static shifts. The MT sounding curve is shifted vertically so that the high frequency part of the MT curve agrees with the TEM curve. The low-frequency MT curves then provide an undistorted picture of the deep resistivity section (Jones, 1988).

## 2.3 Inversion theory

Geophysical data are modelled and interpreted in terms of subsurface parameters in two ways: a direct way, known as forward modelling, and an indirect way, known as inverse modelling. In the forward modelling, the response functions are estimated from the model parameters of the subsurface. On the other hand, in the inverse method, a guessed initial model of the subsurface is assumed and a theoretical geophysical response is computed for the assumed model and compared with the observed data. This process is repeated for various models through an iterative process until a minimum difference between the computed and the observed response is achieved. The result is the statistically best solution with conclusive estimates of the model parameters, and it groups the parameters into well determined parameters and poorly determined ones and calculates how the estimates may be interrelated. It also indicates which data points contain relatively important information necessary to resolve the model parameters.

The forward algorithm for MT is the standard complex impedance 1D recursion algorithm. For TEM, the forward algorithm uses standard recurrence relationships to calculate the kernel function for the vertical magnetic fields, due to an infinitesimal grounded dipole with harmonic current on the surface of a horizontally layered earth (Árnason, 1989; Ward and Hohmann, 1987).

The inversion algorithm used in TEMTD is the Levenberg-Marquardt non-linear least square inversion described by Árnason (1989). The misfit function is the root-mean-square difference between measured and calculated values ( $chisq$ ), weighted by the standard deviation of the measured values. In fitting values, it is a matter of choice for the user whether to use apparent resistivity or measured voltages.

Further on in the program used for inversion (TEMTD), it has the capability of smoothing models. This occurs with respect to resistivity variations between layers (actual logarithm of conductivity) and layer thicknesses (actual logarithm of ratios of depth to top and bottom of layers). Damping is done on “first derivatives“ and “second derivatives“. The former counteracts sharp steps in the model while the latter counteracts the oscillations in the model values (log scale). The minimised function in this process is the weighted root-mean-square misfit ( $chisq$ ), and also the “potential“:

$$Pot = chisq + \alpha \cdot DS1 + \beta \cdot DS2 + \gamma \cdot DD1 + \delta \cdot DD1 \quad (10)$$

DS1 and DS2 are the first and second order derivatives of log-conductivities in the layered model, and DD1 and DD2 are the first and second order derivatives of the logarithms of the ratios of layer depths. The coefficients  $\alpha$ ,  $\beta$ ,  $\gamma$  and  $\delta$  are the relative contributions of the different damping terms and are specified by the user.

## 2.4 Reykjanes high-temperature geothermal field

The Reykjanes peninsula is situated on the southwest tip of Iceland. The region has several high-temperature areas. This report discusses results from 1D joint inversion of TEM and MT data taken from the Reykjanes high-temperature area (Figure 6), which is situated on the outer Reykjanes peninsula along with Eldvörp and Svartsengi to the east. These high-temperature areas are situated directly in the path where the Mid Atlantic Ridge comes ashore.

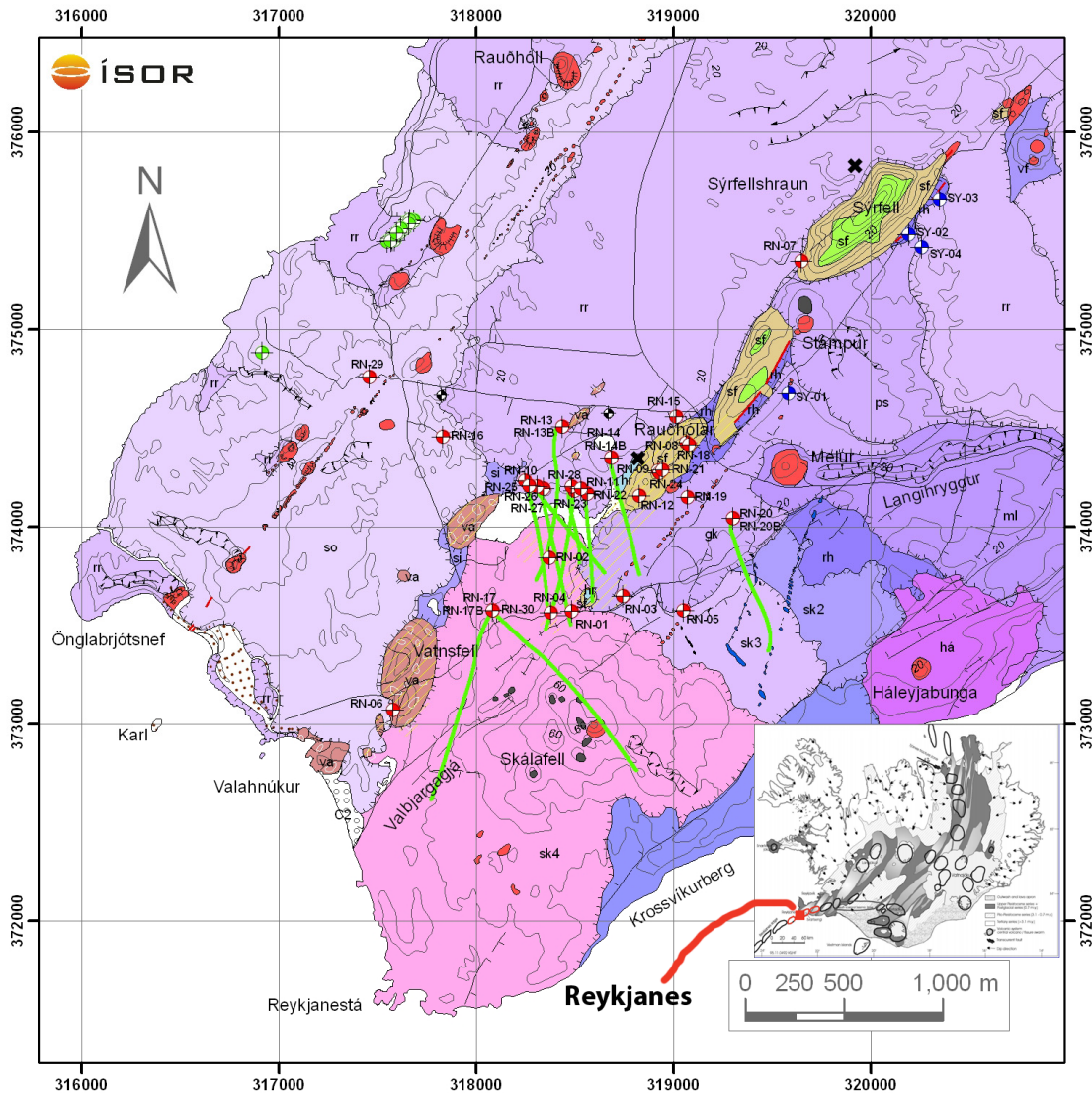


FIGURE 6: Geology of the Reykjanes high-temperature field (modified from ISOR database)

### 2.4.1 Geology and tectonics of the Reykjanes system

The history and geology of the Reykjanes system is well established by a lot of research and studies done in the area. Sigurdsson (2010) gave a detailed overview of the geology and surface manifestations of the Reykjanes high-temperature field, partly based on some findings/work by Fridleifsson and Albertsson (2000). Figure 6 shows the geology and the surface manifestations of the area. Sigurdsson (2010) described it as being entirely covered by sub aerial lavas of Holocene age, whereas hyaloclastites ridges of late Pleistocene age poke the lava fields, with the same NE-SW strike as the volcanic crater rows, faults and fissures. Parts of the hyaloclastite ridges and lava fields are hydrothermally altered,

and are centred within manifestations of fumaroles, mud pools and hot springs. The youngest fissure eruptions date back to 1226 at the crater row Stampar on the northwest side of Reykjanes, while the 2<sup>nd</sup> youngest is about 2000 years old. Within this fissure zone, at least 4 volcanic eruptions occurred in the Holocene period. Sigurdsson (2010) further points out the older fissure zone situated on the southeast side of Reykjanes, close to the Skálafell fissure zone. Frequent movement of faults and fissures over time have reactivated the hydrothermal manifestations, which are mostly located between these two eruptive zones.

The peninsula experiences high seismicity, characterised by normal faulting on northeast striking planes or strike-slip on north or east trending planes (Einarsson, 1991). Seismicity mostly occurs at between 1 and 5 km depth and the oblique motion appears to cause bookshelf deformation, whereby parallel N-S trending, right-lateral strike-slip faults accommodate the overall left-lateral transform motion.

Previous geophysical work using DC Schlumberger methods in the 1970s revealed a continuous elongated zone of resistivity below  $6 \Omega\text{m}$  (low-resistivity zone) in the Reykjanes peninsula (Georgsson, 1981). Later surface resistivity surveys include TEM and most recently MT. The measurements delineated a low-resistivity area interpreted as altered rocks due to high temperatures (see Sigurdsson, 2010 and references therein). The interpreted low-resistivity sheet has an aerial extension of around  $11 \text{ km}^2$  at 800 m depth (Figure 7). A profile with MT and TEM measurements along the Reykjanes peninsula in 2008 revealed resistivity anomalies at depth under the Reykjanes high-temperature field, as well as other locations connected with geothermal activity (see Sigurdsson, 2010 and references therein). In 2010, more MT measurements were done in all TEM measured locations in the area. The results from 1D joint interpretation of the TEM and MT soundings showed the existence of a low-resistivity body down to 8-10 km's depth under the high-temperature field in Reykjanes.

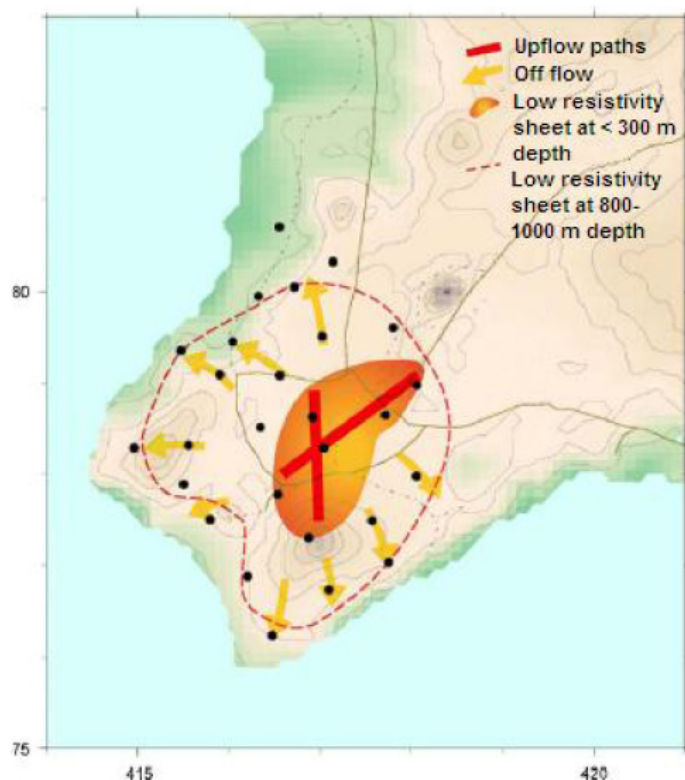


FIGURE 7: Areal extent of the low-resistivity body at 800 m depth (Sigurdsson, 2010)

Earlier exploration dates back to 1956 when the first well was drilled to 162 m depth, reaching temperatures of up to  $185^\circ\text{C}$ . It was soon discovered (Björnsson, 1971) that the salinity of the geothermal fluid was from seawater which made up the brine extracted in the area.

The Reykjanes geothermal field went through many developmental stages. From the 1970s through to the 1990s, it was mainly exploited for a salt factory. In the late 1990s, further investigations resulted in the drilling of well 10, and plans for developing the field for electrical generation. The power plant came online in May 2006, generating 100 MWe from two 50 MWe double flow turbines, with seawater cooled condensers (Sigurdsson, 2010).

### 3. FIELD PROCEDURES AND DATA ACQUISITION

It is essential to record field procedures as they differ in application and configuration from country to country and also differ depending on the aim of survey. The procedures and configurations used in my discussion are entirely based on ISOR's (Iceland GeoSurvey's) configurations and standards, applied to geothermal exploration in Iceland.

Before deploying MT and TEM equipment and their components, it is important to make sure that they are properly tested and checked. This section of the paper is written based on practical hands on experience on data acquisition and equipment setup of both TEM and MT during a field campaign at Hágöngur/Thórisvatn.

At this point, the location of all sounding stations had been planned and mapped out such that the factors outlined below were avoided and/or minimised to have a better chance for acquiring quality data.

- 1) *Topography*: EM soundings generally require setup on regular terrain.
- 2) *Power lines & electrical fences*: Soundings must be located at least 500 m away from these objects to avoid uncontrolled high frequency signals.
- 3) *Accessibility*: Preferably accessible by vehicle. Mainly to save time.
- 4) *Seasons*: Avoid seasons that bring thunderstorms which generate a lot of disturbance by injecting high-frequency and noisy signals into the area.
- 5) *Human population and environmental factors*: Movement of people and vehicles can be a source of noise in the area and, furthermore, people have the tendency to interfere with the stations in a more drastic manner. Landforms such as rivers and lakes and even geothermal manifestations are not favourable places at which to acquire quality data.

#### 3.1.1 MT setup

Prior to an MT survey and before setting up an MT sounding (Figure 8), it is necessary that calibrations be done on MT equipment. During this field campaign, calibrations were done before the setup of the MT soundings. Three control units consisting of two 5 channel/component control units and one 2 Channel/component control unit were used (Figure 9). The process is delicate, particularly in dealing with the magnetic coils which require care when handling. They were placed parallel and 3 m from each other (Figure 9a). Calibration involved establishing communication between the field computer and the control unit, thus, all necessary components mainly coils, global positioning system (GPS) and ground electrode had to be connected. A start-up file containing information like gains, filters, acquisition time and calibration was loaded onto the field computer using the SSMT2000 program. At this stage, the status of the data acquisition unit and its components was visually inspected before it was instructed to calibrate and store the start-up file onto a flash disk. During the same process all units were time synchronized using GPS satellites.

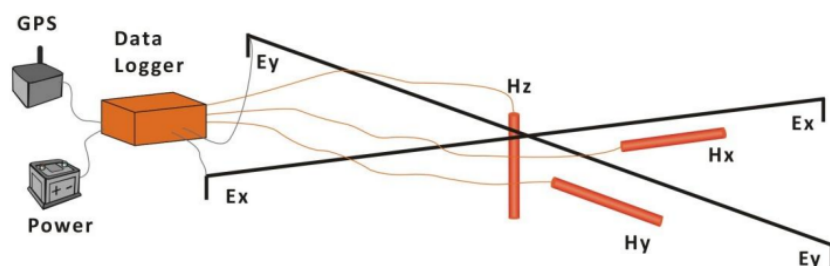


FIGURE 8: MT layout (Flóvenz et al., 2012)

To reduce the noise, particularly local cultural noise, a remote station was set up some tens of kilometres away from the survey area during data acquisition. The idea is that the magnetic field generally is the same over a large area and local cultural noise recorded at MT stations may not be recorded at the remote station. Therefore, remote stations are needed to correct for bias in the MT data as the noise part of the signals is not coherent at the two sites.



FIGURE 9: MT a) Laying out coils 3 m apart in preparation for calibration; b) Setting up recorders for calibration; c) Showing computer cable connection to recorders; d) Recorder placed facing north; e) Recorder placed in plastic bag covering; f) Planting of electrode into the earth; g) Placing bentonite on to the ceramic bottom of the electrode; and h) Burying magnetic coil component with precise orientation (N-S and E-W)

When setting up an MT sounding, the location of the station was scouted before choosing the area with a surface which typically had no more than 20 degrees of slope and was free from factors mentioned earlier. In this survey, a 5 channel MT data acquisition system (MTU-5P) from Phoenix Geophysics was used. The MT setup is made up of a data recorder, 5 non-polarising electrodes, a GPS, a 12 V battery, a flash memory card, three induction coils (telluric), a clinometer/ Brenton compass, levelling devices (3 bubbles), spades, a plastic bag for the recorder, a tripod and co-axial cables.

The typical layout for an MT sounding is shown in Figure 8, which shows the electrodes aligned in magnetic NS and EW directions, and the magnetic components in an orthogonal manner. It is customary to have the x-direction pointing to magnetic north. The recorder is placed at the centre and is usually facing north.

Firstly, the centre of the site is determined using a levelling device dropped from the tripod. The tripod is used to set up the bearings, marked with stakes by which the electrode cables are fastened to the centre pole and are moved, accordingly, to their respective placing (Figure 9).

The four electrode dipoles are buried 50 m away from the centre and 40 cm deep. The porous ceramic base of the electrode is coated with bentonite (Figure 9g) and buried with electrolytic solution salt. These measures enhance the conduction between the electrode and the ground.

The magnetic coils are extremely sensitive to noise from wind, people walking, or trucks, thus they are buried to prevent movement. The magnetic coils are precisely aligned N-S and E-W, respectively, making sure that they are properly levelled (Figure 9h) and the horizontal coil is buried upright, levelled at a 90° angle.

### 3.1.2 MT data acquisition

At each MT station, five measurements (channels) are recorded. They are the magnetic field in the two horizontal directions and in the vertical direction, and the electric field in the horizontal directions. In the MT method, the natural fluctuations of the earth's magnetic field are used as the signal source. Those fluctuations induce currents in the ground which are measured on the surface ( $E_x$  and  $E_y$ ). The magnetic field is measured in three orthogonal directions ( $H_x$ ,  $H_y$  and  $H_z$ ) (Figure 8).

The electric and magnetic fields are measured as a function of time. The four channels are  $E_x$ ,  $E_y$ ,  $H_x$ ,  $H_y$ . From basic physics, the electric field in the x direction ( $E_x$ ) should correlate with the magnetic field in the y direction ( $H_y$ ), and similarly  $E_y$  correlates with  $H_x$ .  $H_z$  is recorded to give information about the electric strike.  $E_x$ ,  $H_y$ ,  $E_y$  and  $H_x$  can be used to get information about the subsurface resistivity.

The data are synchronized with GPS signals and by comparing these data with another station's simultaneous recording, noise can be identified and reduced. This method, known as "remote referencing," allows the data at one station to be compared to data at another station, recorded at exactly the same time, and compared for coherency. Any non-coherent data are thrown out and are considered to be noise. This greatly improves data quality. Recording at each station takes 6-18 hours, depending on signal strength and survey parameters.

For a homogeneous or layered earth the electrical field is induced by (coherent with) its orthogonal source magnetic field (i.e.  $E_x$  correlates with  $H_y$ , and  $E_y$  with  $H_x$ ). For more complicated resistivity structures, these relationships become more complex. The magnetic field was measured with induction coils and the electrical field by a pair of led-chlorite filled electrodes. The MT instruments used are from Phoenix Geophysics in Canada (2009), MTU type, and can measure the MT signals in the frequency range from about 400 Hz to 0.0000129 Hz.

In each sounding the MT units were deployed for recording and picked up the following day, giving about 20 hours of continuous time series. The short-period MT data (high frequency) mainly reflect the shallow structures due to their short depth of penetration, whereas long period data mainly reflect the deeper structures. The MT method has the greatest exploration depth of all resistivity methods, some tens or hundreds of kilometres, depending on the recorded periods, and is practically the only method for studying deep resistivity structures. In this survey, the exploration depth of the MT soundings was around 30 km, but varied considerably depending on resistivity and in particular on data quality.

### 3.1.3 TEM setup and data acquisition

Because of static shift problems in MT data in volcanic geothermal fields, care is taken when conducting TEM surveys so that they are placed at the same spot as the MT sounding (within 50-100 m). TEM equipment owned by ISOR was used for this and consisted of a PROTEM receiver and a TEM57-MK2 transmitter from Geonics, Ltd. It also had a power module (current booster), a small receiver loop (100 m<sup>2</sup>), a big receiver loop (5613 m<sup>2</sup>) and a reference cable. To produce higher and stable currents (25 A) ISOR uses a 5 kV generator.

Before setup for TEM, it is imperative to synchronize the crystal clocks in both the transmitter and the receiver. Usually they are heated up for half an hour or more. While waiting for the synchronization to complete, the TEM layout can be done. First the square transmitter loop is laid out; the size of loop is dependent on the depth of interest (to probe a depth of 1000 m, 300×300 m<sup>2</sup> is sufficient). Then the centre of the transmitter loop is marked for layout of the 10×10 m receiver loop.

Before data acquisition, current from the transmitter is sent through the transmitter loop and measured at low frequency (2.5 Hz). Extra current needed for the process is taken from the power modules, included among the equipment. Current values are registered on the transmitter when it becomes stable. Turn of time (TOT) is measured in micro-seconds at high frequency (25 Hz). This information is required in order to calibrate the receiver before measuring TEM data.

The transmitter current, usually 18-22 A, is transmitted at a high frequency of 25 Hz and a low frequency of 2.5 Hz. For each frequency, 20 measuring time gates were evenly spaced on a log-scale from 0.09-7 ms for the high frequency, and 0.9-70 ms for the low frequency, after current turn off. Repeated transients were stacked and stored in the computer memory of the receiver and later downloaded to a personal computer, ready for further processing.

## 4. DATA PROCESSING AND INVERSION

This section of the report describes the process and steps involved in preparing the MT and TEM raw data, using various programs used by ISOR. Processing of MT data involved the use of SSMT2000 software by Phoenix while the TEM raw data were processed using an in-house program TemX, which was developed by ISOR (Árnason, 2006a). SSMT2000 is a Windows-based software used in a Windows XP platform, while the TemX is a UNIX based program.

TEM and MT data used in this section were borrowed from HS Orka for this project exercise and consisted of 17 TEM soundings and 17 MT soundings. The measurements of TEM and MT data were made in the years 2008, 2010 and 2012. For joint inversion purposes, the TEM and MT had to be paired so they were measured approximately in the same location to give better results.

Inversion of both TEM and MT was done using TEMTD (Árnason 2006b), developed by ISOR. The program has the capability of inverting both TEM and MT, independently or even jointly.

### 4.1.1 Processing of MT data

Raw data from MT were imported into SSMT2000 where the calibration files and also the remote station data were used for processing. The digitally recorded times series were Fourier transformed from the time domain into the frequency domain, then the robust processing method provided by the SSMT2000 was used to calculate the auto and cross powers.

The output files, consisting of average cross and auto powers, were imported into MTEditor (program from Phoenix) where manual editing was done. Manual editing is only necessary if a visual inspection of the data is unsatisfactory in the eyes of the experienced geophysicist. The processed sounding is saved as a standard EDI file format which can then be used as an input file for the inversion process.

The MT data must go through a series of steps following the above, where conversion of the EDI file to a UNIX format is required in order to invert the apparent resistivity and phase contained in the auto and cross powers. The following steps were followed:

- 1) Input files RKN018.**mtb** and RKN018.**mtl** are automatically formed by the MTEditor which are used to produce the file RKN018.**mpk**.
- 2) Using MT-Editor, we converted for EDI (universal data standard for MT) using RKN018.**mpk** file. The file, at this stage, will have the extension **.edi** which is in ASCII format.
- 3) The next step is to convert the file in ASCII format to BINARY format so that the **.edi** can be used in UNIX. This step is required because all programs used for inversion were developed in the UNIX background. The conversion is done using the command **dos2unix** which is executed in terminal mode in UNIX.
- 4) **spect2edi** command is then executed on the resulting file from the last step, where the file format is rearranged and calculations of various MT parameters and GPS coordinates are converted from degrees to wgs84. The product from this step is a standard EDI file format with the extension **.EDI**.

The file produced (RKN018.**EDI**) at the end of this process is now the input for TEMTD which is a UNIX based program used to invert MT and TEM data. Figure 10 shows a typical processed MT data, generated using the TEMTD command **edi2ps**.

### 4.1.2 Processing TEM data

TEM data measured by the PROTEM-D3 receiver were extracted and loaded into TemX program for visual inspection and editing. TemX calculates averages and standard deviations for repeated transient voltage measurements and calculates late time apparent resistivity as a function of time. These are

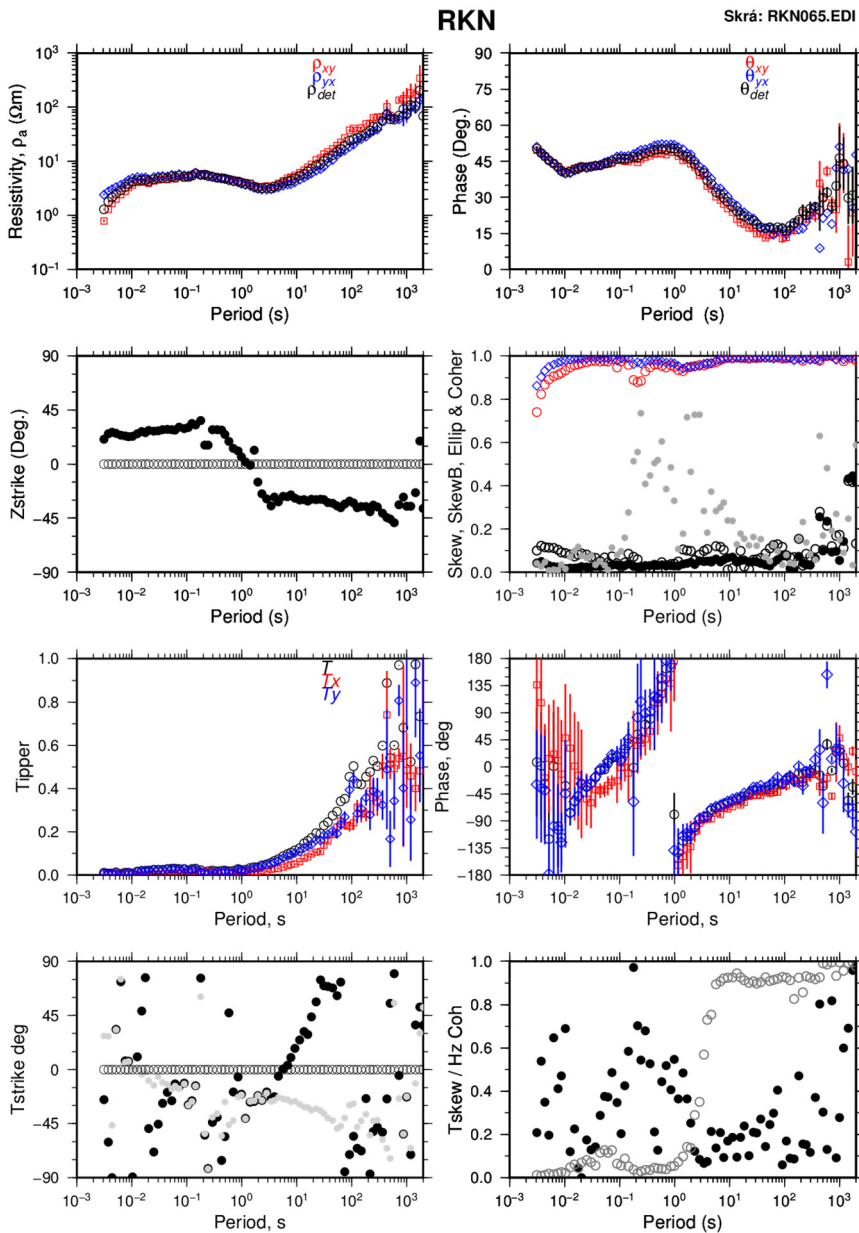


FIGURE 10: Processed MT data: The top row shows apparent resistivity denoted by  $\rho_{xy}$  (red) and  $\rho_{yx}$  (blue) which is also depicted in the associated Phase diagram to the right; The  $\rho_{det}$  (black) dots denote the determinant invariant; The second row of diagrams shows the Z-strike (Swift angle) denoted by black dots on the left side; on the right is shown the coherency dots in red and blue for  $\rho_{xy}$  and  $\rho_{yx}$  respectively; The black dots depict skew and the grey dots are the ellipticity; The bottom two rows of diagrams show various forms of Tipper data

displayed visually using a graphical-user interface (GUI); the program is also user interactive where the outliers or noise readings can be masked out by the click of a mouse. For my project, 8 TEM soundings were processed using TemX while the rest were already processed INV files. To process TEM data using TemX, the file is loaded using TemX in a UNIX terminal.

Upon loading TEM data, the turn off time and the drift values recorded in field note books are given where necessary. This is needed to correct for turn-off time and drift time recorded off the PROTEM-D3 transmitter during the survey. TemX displays the TEM data, as shown in Figure 11, where on the left, the transient voltages are plotted versus time, and the right shows apparent resistivity plotted versus time. In the apparent resistivity plot, the blue dots represent the high frequency data recorded at early times, while the red and green dots are the late time data recorded at low frequency.

All masking is done at the voltage plot where stacking of voltages at the same time is performed. Once satisfied, the TEM data file header is modified, by adding information about the data. Information such as coordinates of the sounding, elevation, personnel involved in the survey, site of the sounding, sounding name and the datum used at that time are then inserted. For this case, the datum used was UTM-WGS84. The TEM data is now complete and saved as an .INV file which will be the input file to the program TEMTD.

### 4.2 Inversion of TEM and MT data

Inversion of TEM and MT data was done using the TEMTD program. TEMTD performs 1D inversion with horizontal layered earth models or Occam inversion of central-loop Transient Electro-Magnetics (TEM) and Magnetotelluric (MT) data. It can be used to invert either TEM or MT data, or jointly invert both TEM and MT data, by which the best static shift parameter for the MT data is determined. The program assumes, for TEM data, a source loop of square shape and that the receiver loop is at the centre of the source loop. Waves forms of the current are assumed to be half-duty bipolar semi waves (equal current-on and current-off segments), with exponential current turn-on and linear current turn-off. For MT data, the program assumes standard EDI for impedance and/or apparent resistivity and phase data. The program runs under UNIX/LINUX operating systems and is written in ANSI-C. It uses the gnuplot graphics program to display graphics from the inversion.

For this report, at the start only TEM data were inverted using 1D (layered earth) Occam (minimum structure) inversion; final models (.plo files) were set aside for use in the joint inversion of TEM and MT. During this process, the rotationally invariant determinant apparent resistivity and phase of the MT and TEM soundings were inverted. Figure 12 shows a typical result of such inversion. The best estimate of the shift parameter for this sounding is  $S = 0.686$ , i.e. the MT apparent

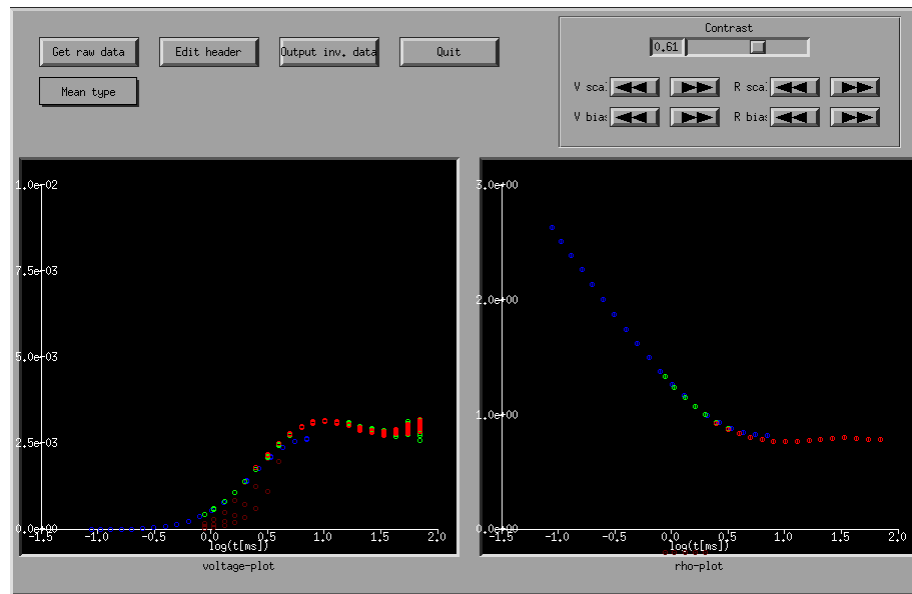


FIGURE 11: TemX GUI used to visualize TEM data and edit outliers/noise

The program assumes, for TEM data, a source loop of square shape and that the receiver loop is at the centre of the source loop. Waves forms of the current are assumed to be half-duty bipolar semi waves (equal current-on and current-off segments), with exponential current turn-on and linear current turn-off. For MT data, the program assumes standard EDI for impedance and/or apparent resistivity and phase data. The program runs under UNIX/LINUX operating systems and is written in ANSI-C. It uses the gnuplot graphics program to display graphics from the inversion.

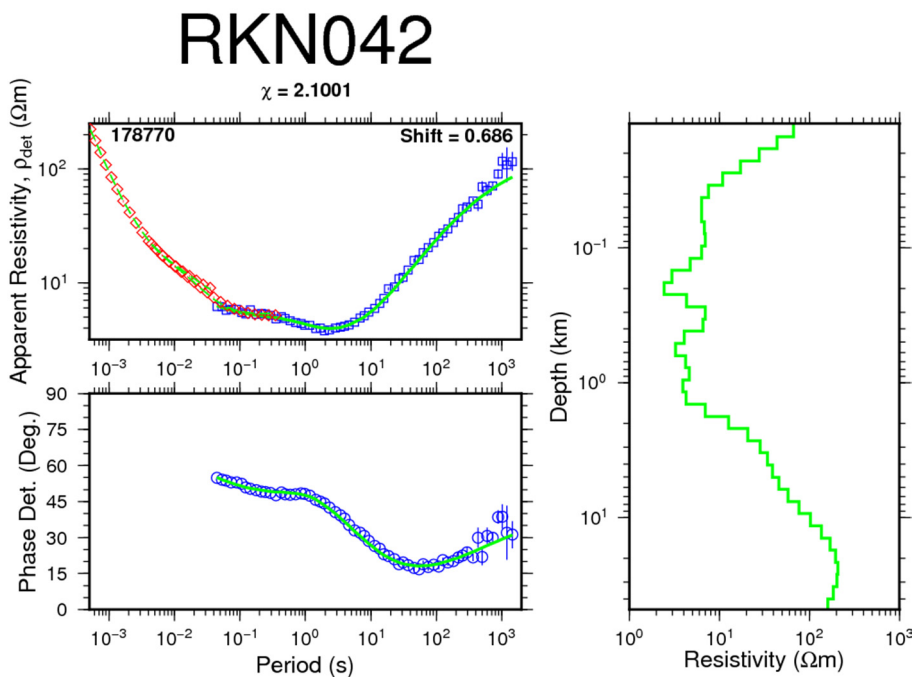


FIGURE 12: A typical result of 1D joint inversion of TEM and MT soundings; red diamonds: TEM apparent resistivities transformed to a pseudo-MT curve; blue squares: measured apparent resistivities; blue circles: apparent phase derived from the determinant of MT impedance tensor; light blue symbols to the left of the green curve: data not used in the inversion; green lines: on the right are results of the 1D resistivity inversion model and to the left are its synthetic MT apparent resistivity and phase response; vertical blue line: error bars

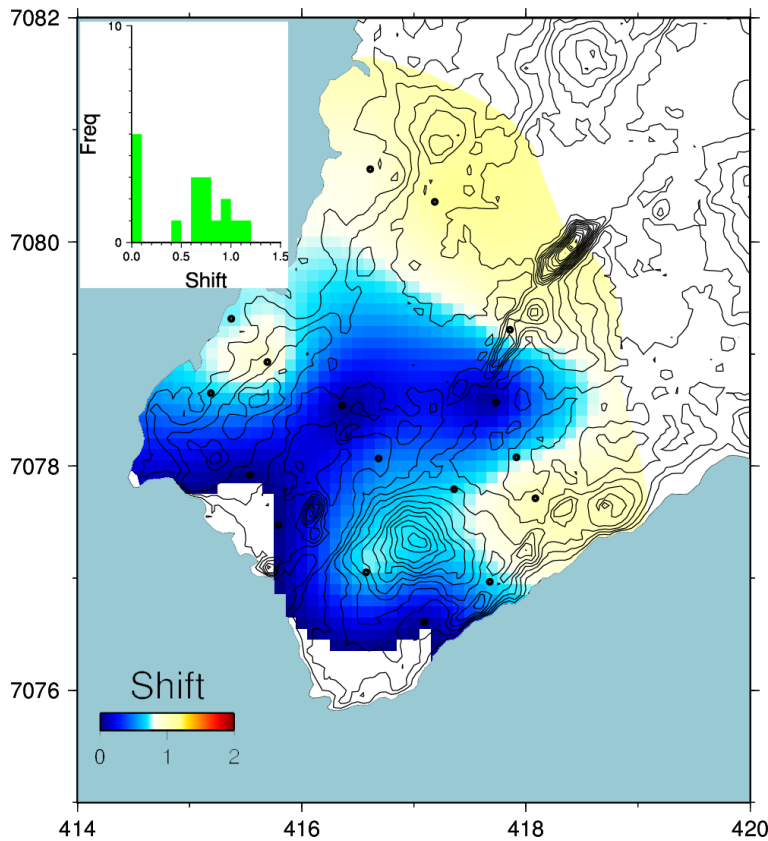


FIGURE 13: Spatial distribution of static shift parameters for the determinant apparent resistivity in the Reykjanes area; black dots denote TEM and MT sounding locations

resistivity has to be divided by 0.686 to be consistent with the TEM sounding. In Figure 12, the TEM data were plotted as a function of the period (T) by using the transformation  $T = t/0.2$  (Sternberg et al., 1988) which differs from what happens in the inversion of TEM only.

A histogram of all shift multipliers for all 17 soundings is given in Figure 13 as an insertion. It is seen that they are in the range 0.1-1.2, and that the static shift multipliers lower than one are more common than those higher than one. Shifts lower than 1 are within the vicinity of surface manifestations. The shift values greater than 1 are located further away from the low-resistivity anomaly and the surface manifestations (Figure 13). It is, therefore, important to calculate and map out the shift distributions.

### 5. RESULTS AND INTERPRETATION

From the 1D joint inversion of TEM and MT data, associated programs written by ISOR were used to generate: cross-sections, iso-resistivity maps, shift maps, rose diagrams and induction arrows, which are given in the Appendix section of the report (Verave, 2013). Due to technical issues, rose diagrams, induction arrows and Tippers were not produced. In all, 17 TEM and MT soundings were jointly inverted. Four profiles, shown in Figure 14, were used to extract cross-sections to a depth of about 20 km. The map also shows surface manifestations and wells used to correlate with subsurface resistivity.

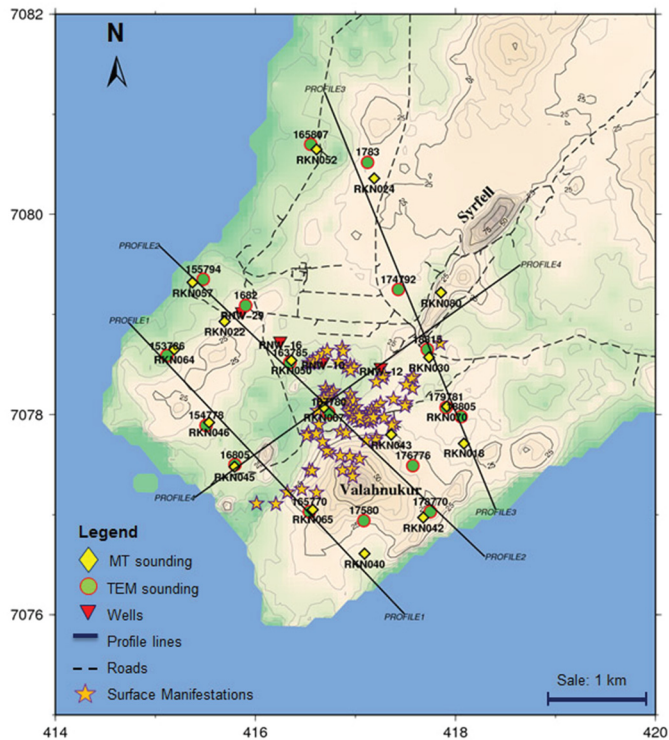


FIGURE 14: Locality map of TEM and MT soundings

### 5.1 Resistivity cross-sections

Profile 1 runs approximately 3.5 km NW-SE and is situated in the southwesternmost part of the Reykjanes geothermal field. Figure 15 shows two cross-sections taken from this profile where five TEM and MT soundings were used. Cross-section A reveals subsurface resistivity distribution down to 5000 m. A low-resistivity layer is well defined in the upper most part of cross-section A, spanning from 0 to 1800 m depth below sea level (b.s.l.), with resistivity values ranging from 1 to 10  $\Omega\text{m}$ . The lowest resistivity value of 1  $\Omega\text{m}$  was seen below MT sounding RKN046 at a depth of 500-1000 m. The appearance of the conductive cap of low resistivity is consistent with previous resistivity surveys which observed a continuous homogeneous low-resistivity anomaly in the Reykjanes field (see Sigurdsson, 2010 and references therein). Beneath this conductive cap below 1800 m, we see a gradual increase in resistivity down to about 4000-5000 m b.s.l. where the subsurface becomes more resistive. Resistivity values of up to a 100  $\Omega\text{m}$  are observed at this depth.

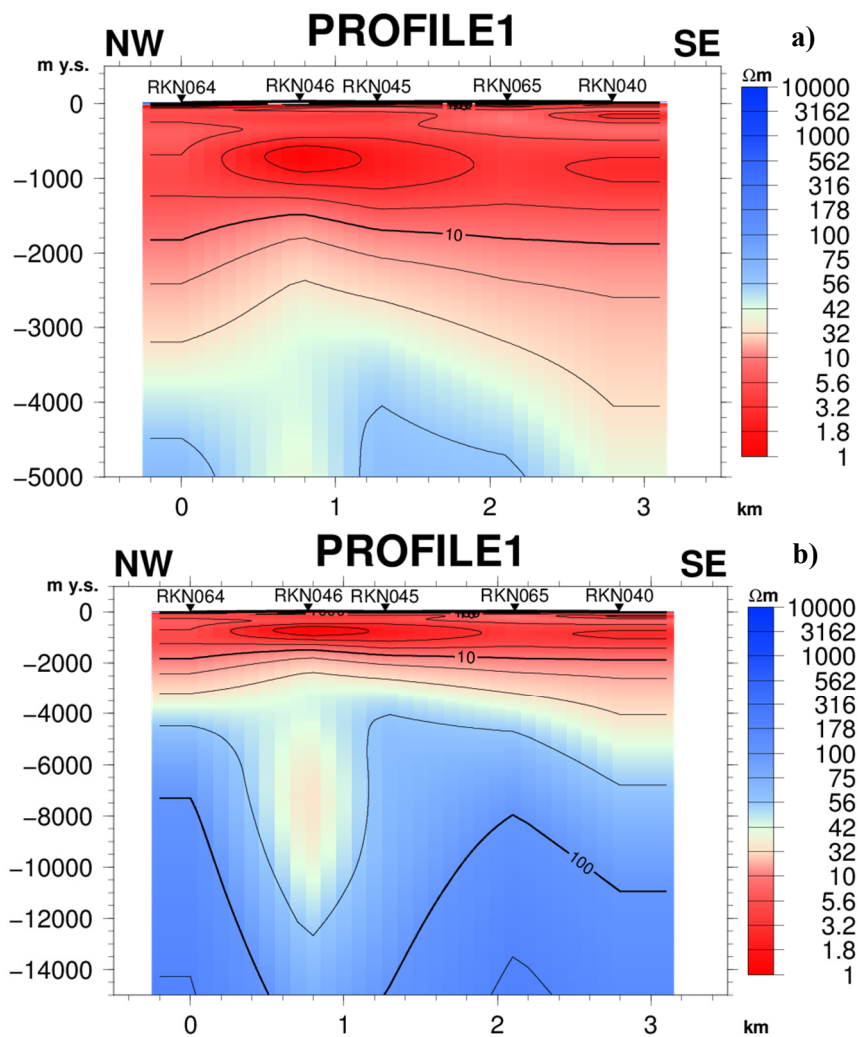


FIGURE 15: Profile 1 showing a resistivity cross-section, a) to a depth of 5000 m; and b) to a depth of 15,000 m

Cross-section B shows the deep resistivity structure beneath profile 1 down to 15000 m, where an anomalous low-resistivity body is prominent. It is directly below MT sounding RKN046 and extends from 4000 to 12000 m, i.e. through the high-resistivity body. The resistivity in this body may be up to 40  $\Omega\text{m}$ . This presumably could be due to low-resistivity alteration minerals that have precipitated in fractures and filling beneath MT sounding RKN46. It is also observed that the conductive cap is thinner in the northwest and broadens toward the southeast (controlled by surface activity).

Profile 2, (Figure 16), runs NW-SE, and is located between profile 1 and profile 3 (Figure 14) and passes through the area of main surface manifestations. It spans across the centre of the high-temperature area, for 3.8 km, including 6 TEM and MT soundings. Cross-section A of profile 2 shows a similar resistivity distribution as profile 1, with a homogeneous low-resistivity cap extending from 0 to 2000 m depth. The lowest resistivity values of 1  $\Omega\text{m}$  was observed beneath MT sounding RKN067 and extends a little southeast directly under MT sounding RKN043 and is encountered at a shallow depth of 200 m and extends to about 800 m. The 10  $\Omega\text{m}$  resistivity contour clearly defines the transition from the low-resistivity zone to increasing resistivity. Cross-section B of profile 2 does not show the anomalous low-

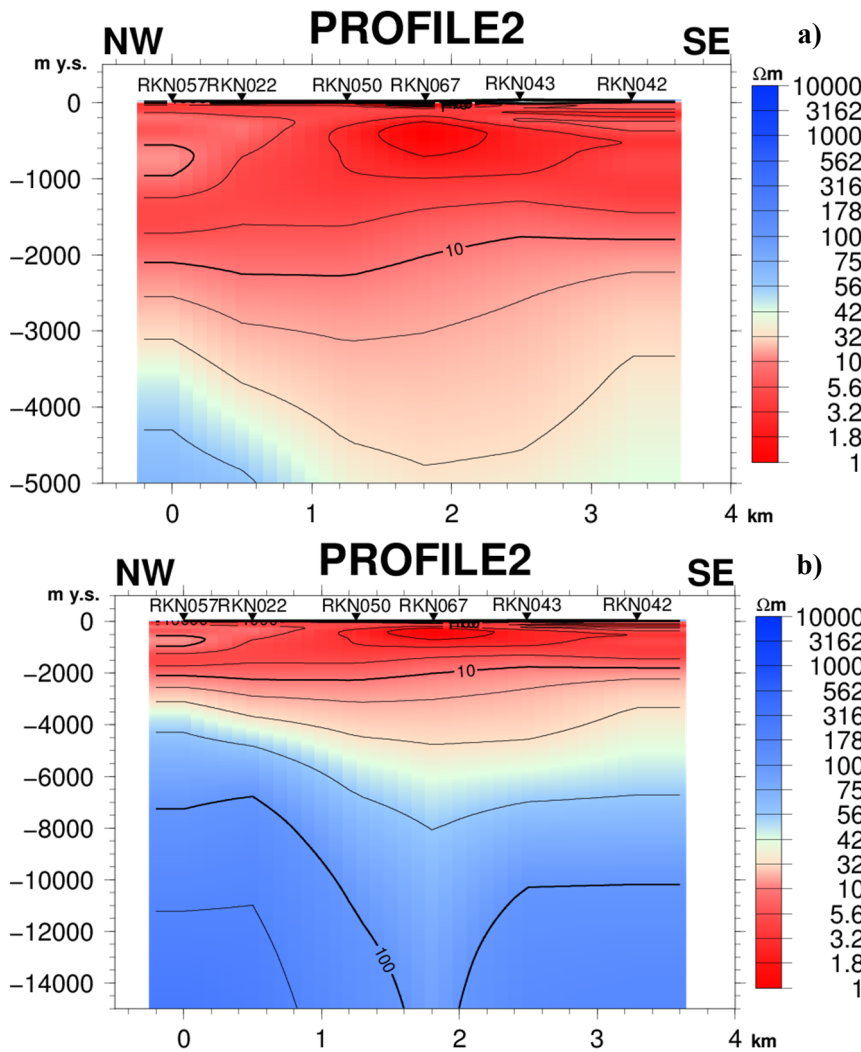


FIGURE 16: Profile 2 showing resistivity cross-section, a) to a depth of 5000 m; and b) to a depth of 15,000 m

resistivity pocket observed in Profile 1. This could be due to the quality of MT data taken from this profile.

Profile 3 (Figure 17) runs also NW-SE, and is located away from the centre of the geothermal field towards the northeast corner. It consists of 6 MT and TEM soundings that make up a profile of more than 4 km in length. The area it covers has little or no surface manifestations. The only manifestations found are located near MT soundings RKN80 and RKN30. Cross section A probes to a depth of 5000 m. The low-resistivity cap at shallow depth is consistent with what has been seen in the previous profiles. However, here the lateral resistivity distribution is not as continuous as observed previously. The resistivity contour shows irregularities and is not well connected laterally. Directly below MT

sounding RKN030, the lowest resistivity of 1  $\Omega$ m was observed; it is laterally continuous towards the southeast of profile 3 between 200 and 1200 m depth. Northwest of profile 3, there is a break in the lateral continuity of low resistivity, caused by the upward appearance of a 10  $\Omega$ m resistivity value.

Cross-section B of profile 3 shows a low-resistivity body at 12,000 m below sea level, similar to that observed in profile 1. The low-resistivity body is encountered at a greater depth than that shown in profile 1 and is directly beneath MT sounding RKN030.

Profile 4 (Figure 18) cuts through the centres of profiles 1, 2 and 3 in a SW-NE direction and covers MT soundings RKN045, RKN067, RKN030 and RKN080 (Figure 14). Cross-section A of profile 4 clearly shows a laterally continuous low-resistivity cap extending from 0 to about 1800 m where the high-resistivity boundary is found. A pocket of very low resistivity is imminent below soundings RKN067 and RKN030, which are situated directly within the area of surface manifestations (Figure 14). Cross-section B shows the subsurface distribution to a depth of 15000 m and reveals a low-resistivity anomaly around the same depth as that observed in profile 3 (12000 m). This low-resistivity anomaly appears to be at the intersection of profiles 3 and 4.

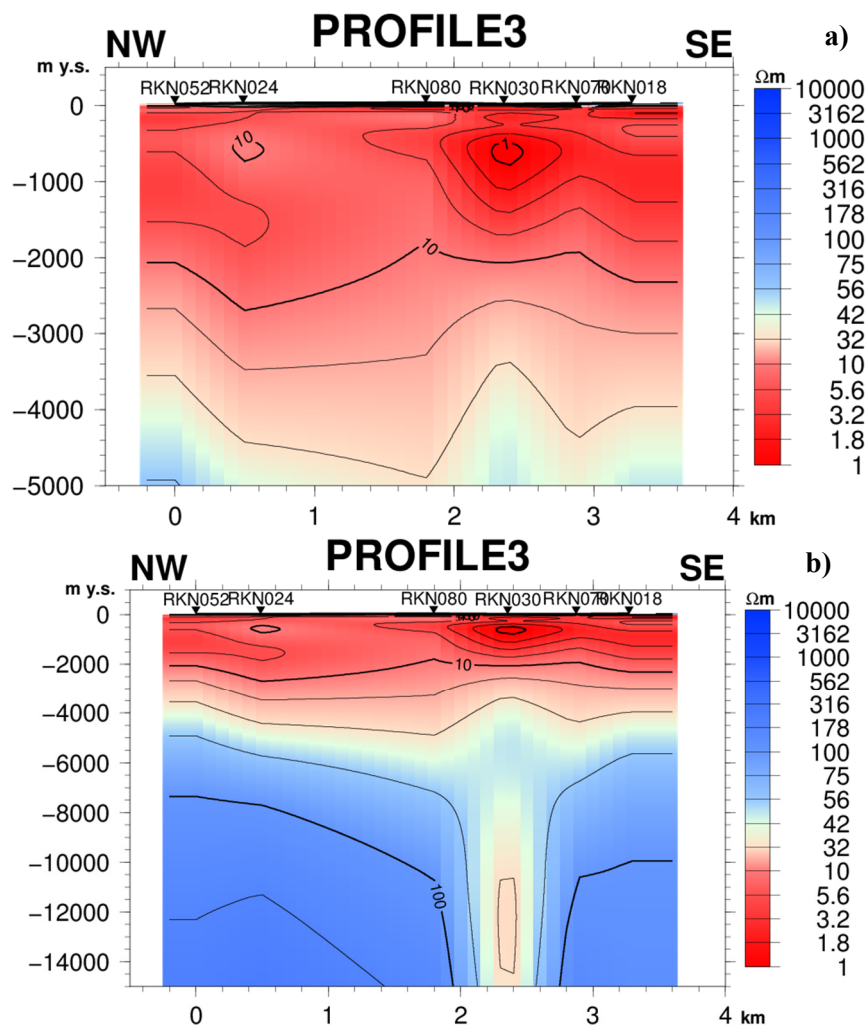


FIGURE 17: Profile 3 showing resistivity cross-section, a) to a depth of 5000 m; and b) to a depth of 15,000 m

## 5.2 Iso-resistivity maps

Figure 19 shows iso-resistivity maps at 500 and 2500 m b.s.l. The areal extent of resistivity at 500 m was interpreted as a low-resistivity sheet which covers the whole Reykjanes geothermal field. Resistivity values range from 1 to 10  $\Omega\text{m}$  with the lowest resistivity found in the central part of the geothermal system and higher resistivity values, mainly towards the fissure swarm in northwest. A resistivity patch of 1  $\Omega\text{m}$  is located directly below sounding RKN030 and it elongates towards the sea in the west where sounding RKN046 is situated (Figure 19a). This may indicate some connectivity below the two soundings. The area of very low resistivity correlates well with the location of surface manifestations.

At 2500 m (Figure 19b) the resistivity is considerably higher with values ranging from 30 to 40  $\Omega\text{m}$ . Lower resistivity values are prominent in the northeast but resistivity increases toward the southwest part of the geothermal field. At this depth, the conductive cap (sheet) has already diminished.

Figure 20 shows the resistivity distribution at 10,000 m b.s.l. High resistivity values of 100  $\Omega\text{m}$  dominate the extent of the geothermal field with two patches of low-resistivity bodies protruding the high-resistivity layer. Judging by the resistivity contours, the two low-resistivity anomalies seem to be connected. A similar connecting trend is seen in Figure 19a. Coincidentally, the two low-resistivity

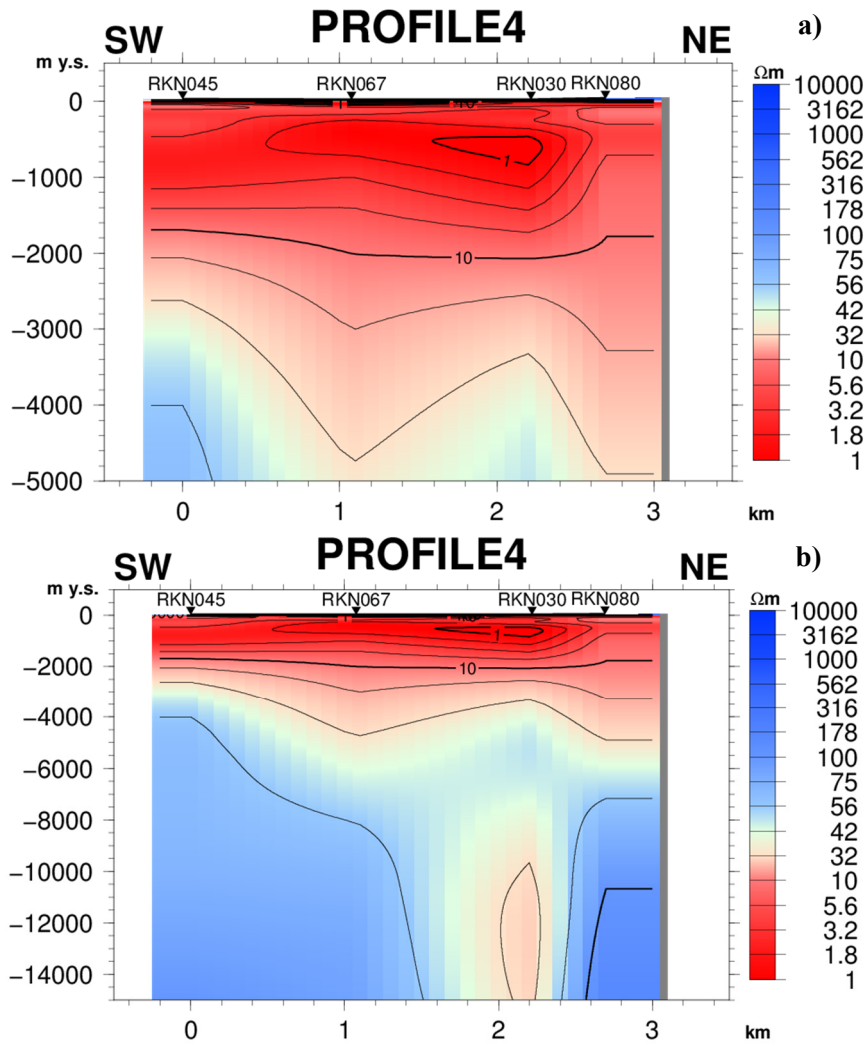


FIGURE 18: Profile 4 showing resistivity cross-section, a) to a depth of 5000 m; and b) to a depth of 15,000 m

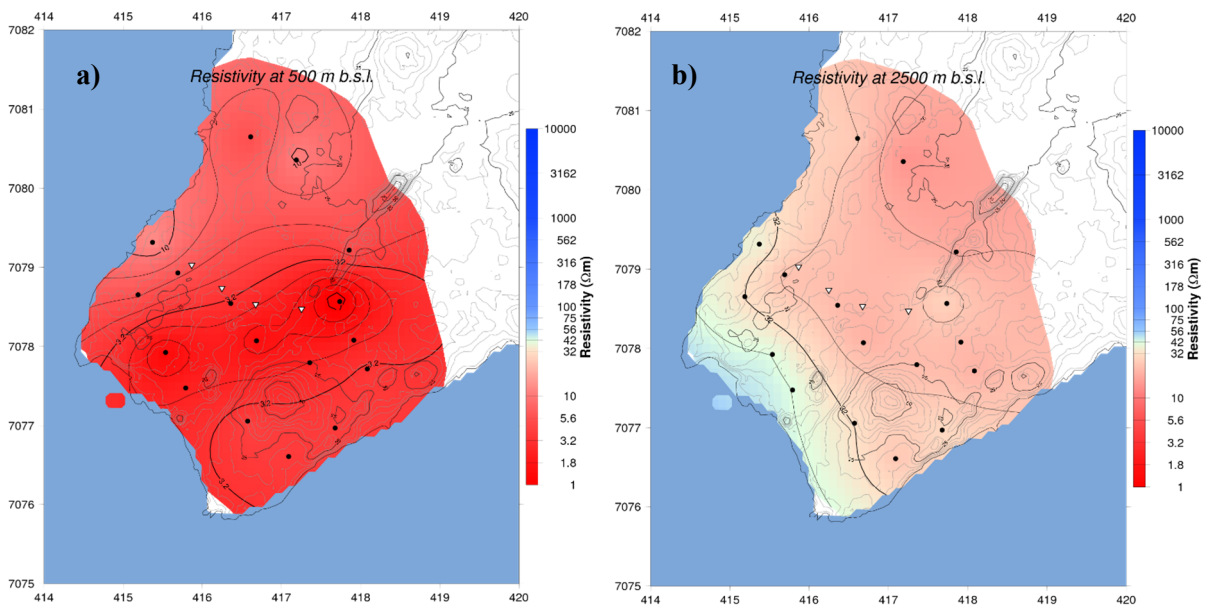


FIGURE 19: Iso-resistivity maps at a) 500, and b) 2500 m b.s.l.

anomalies fall directly beneath soundings RKN030 and RKN046. The low-resistivity anomaly below sounding RKN030 is more prominent than that seen below sounding RKN046. The anomaly could be associated with a heat source at this depth.

### 5.3 Correlating resistivity cross-sections and hydrothermal alteration

For practicing purposes, two cross-sections, from profile 2 and profile 4, were used to show hydrothermal mineral alteration as revealed in cuttings from the boreholes. Well data and information for well 10 were taken from Franzson et al. (2002) and are reliable. Information from wells 16 and 29 were estimates of alteration occurrences at various depths.

Figure 21a shows profile 2 with wells 10, 16 and 29 plotted with their alteration information. Well 10 shows smectite/zeolite from the top and down to 500 m. A thin layer chlorite zone sits below the smectite/zeolite zone with a thickness of 100 m. From 600 to 1100 m, the chlorite/epidote zone is found with epidote/amphibole dominating below 1100 m. The estimated depth and alteration sequences of wells 16 and 29 are similar, only differing in thickness and depth of occurrence. The sequences of the two latter wells are as follows: they start with an unaltered layer at the top followed by a thick layer of smectite/zeolite, a thin mixed-clay layer (100 m). At the bottom of the well, epidote/amphibole dominates.

Using information from well 10, it can be seen that the resistivity cross-section does not correlate sharply with the alteration sequence. While saying that, we can still see

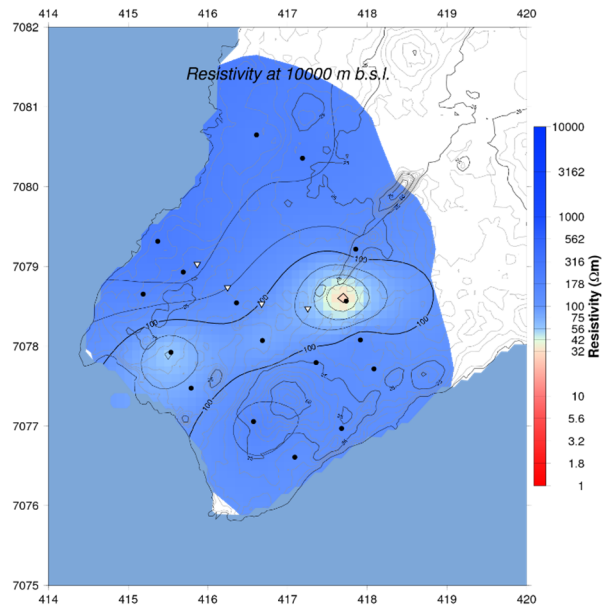


FIGURE 20: Iso-resistivity map showing areal distribution of resistivity at 10,000 m b.s.l.

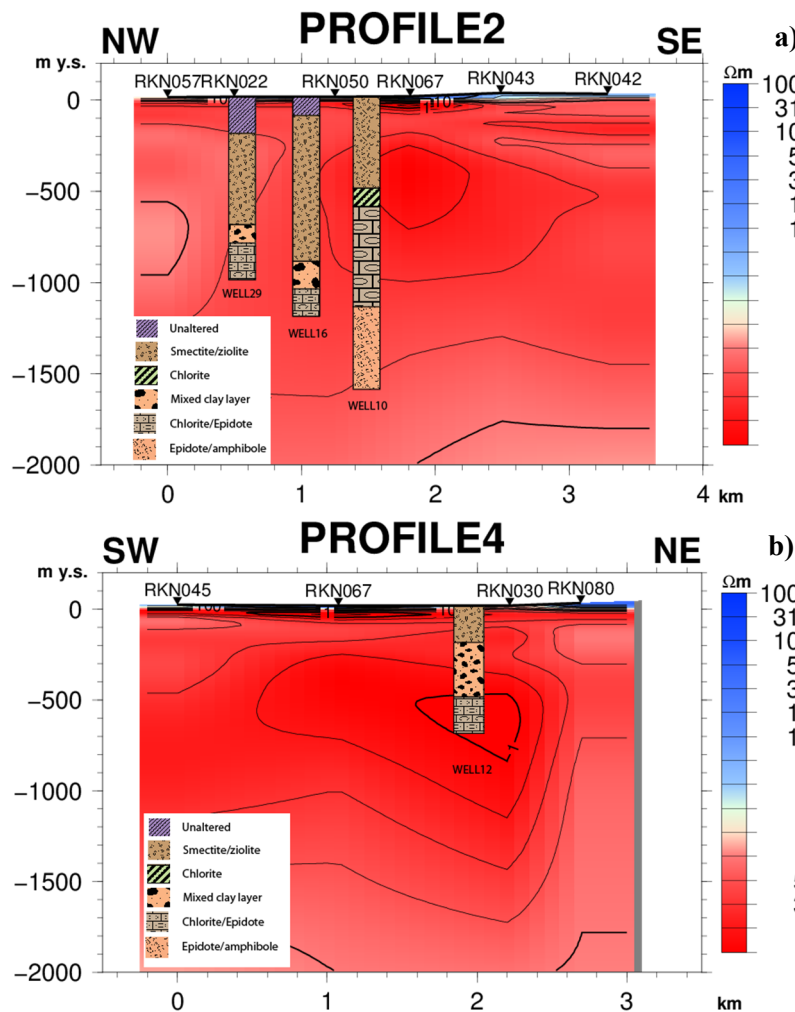


FIGURE 21: Correlation between subsurface resistivity and alteration minerals down to 2000 m; a) Profile 2; and b) Profile 4

some correlation. The smectite/zeolite zone fits well with the resistivity values of 1-3  $\Omega\text{m}$  which are found below soundings RKN050 and RKN067 at a depth of 500 m. A chlorite zone is found within this low-resistivity anomaly, which may infer the transitional boundary of low to higher temperatures. The chlorite/epidote zone is found within the low-resistivity anomaly and extends down and out of the low-resistivity pocket. The colour gradient of the resistivity begins to change at depths where epidote/amphibole are found. Higher resistivity values up to or greater than 10  $\Omega\text{m}$  can be seen and resistive minerals such as epidote and amphibole are dominant. The explanation for the average correlation of the alteration and resistivity distribution can be attributed to the colour pallettes used to display the resistivity distribution and/or are due to the high seawater salinity in the system.

Profile 4 cross-section (Figure 21b) shows well 12 with information of alteration minerals acquired from borehole data given by ISOR. The well penetrates through a region of a low-resistivity patch at a depth range of 500-1600 m. The smectite/zeolite layer is found at resistivity values of 3.5-5  $\Omega\text{m}$ , while the mixed-layer clays are found at a resistivity range of 1-3.5  $\Omega\text{m}$ . The bottom sequence of chlorite/epidote begins at 1  $\Omega\text{m}$  and extends downwards and away from the low-resistivity layer. The alteration and resistivity correlation does not agree very well in this case.

### 5.4 2D layout of profile

All profiles produced were finally arranged in such a way as to give a 2D view of their relative position (Figure 22). The aim was to compare the deep-resistivity distribution and anomaly found in all four profiles at once, and come up with an explanation to questions that might arise from this 2D view. From Figure 22 we see a low-resistivity anomaly at depths of up to 10,000 m in the centre of all three profiles that run through the geothermal field in a NW-SE direction. It is, however, not prominently shown in profile 2 and this could be due to the quality of the sounding above the expected anomaly. Profile 4, in contrast, runs in a SW-NE direction and cuts through the other profiles (as shown by a yellow block), and shows the anomaly at a similar depth but further toward the northeast. There is some linearity about the anomaly which, at depth, is prominent. The low-resistivity anomaly at greater depths may be attributed to the main fractures, running SW-NE, caused by the Mid-Atlantic spreading. The low-

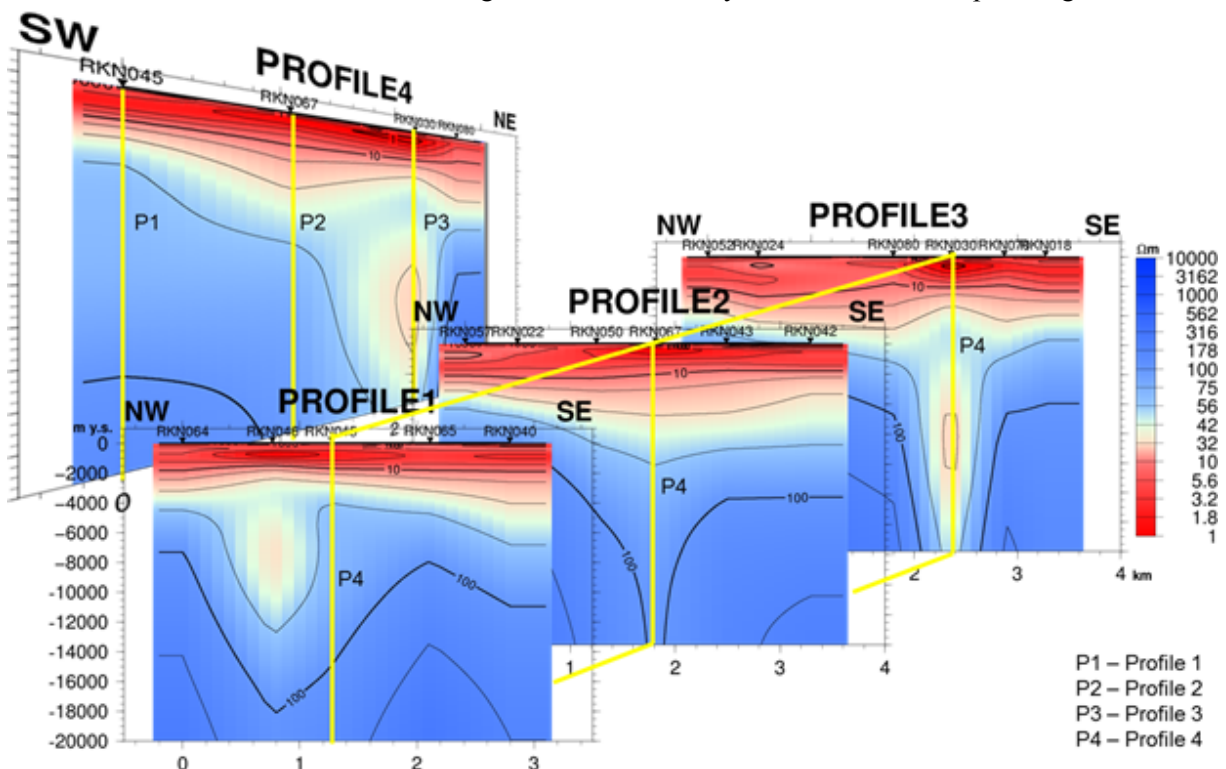


FIGURE 22: 2D layout of a cross-section depicting the deep resistivity distribution of Reykjanes

resistivity values of 10-42  $\Omega\text{m}$  at the anomaly, protrude the much more resistive surrounding formation and the resistivity values may be caused by the appearance of less resistive alteration minerals. In addition, profile 4 shows the same anomaly found in profile 3 and it is much broader than in profile 3; this could be because it cuts through a large portion of the intersection of two fractures described by Sigurdsson (2010).

## 6. DISCUSSION AND CONCLUSIONS

1D joint inversion of TEM and MT data was performed, based on 17 TEM and MT soundings leased from HS Orka for the purpose of my training. The results obtained and interpreted cannot be considered conclusive. Using more data would have helped in giving better results, but the main idea was to become acquainted with the skills and knowledge involved in producing the results presented in this report.

The results of all cross-sections derived from all the profiles were strikingly similar. A homogenous low-resistivity layer exists above a high-resistivity body. The low resistivity is associated with the presence of conductive minerals, such as smectite and zeolite, and the higher resistivity below the conductive cap is caused by resistive minerals such as chlorite, epidote and amphibole. The anomalously low resistivity values are mainly influenced by the seawater salinity present in the geothermal field.

A low-resistivity anomaly, relatively speaking, at deeper parts of the geothermal system, found in profiles 3 and 1, shows resistivity values that indicate the presence of alteration minerals epidote and amphibole, which may have been left behind by the upflow of geothermal fluid. However, it is more likely that this low resistivity is due to different alteration found here in fractures and linings of the walls. This could also mean that the anomaly seen here could be activated by deep fractures where there is good permeability. This is also evident in the iso-resistivity map taken at a depth of 10,000 m b.s.l.

In conclusion, the application of 1D joint inversion of TEM and MT data to detect and delineate geothermal resources is evidently supreme. The results from 1D joint inversion of TEM and MT data can be correlated with the main parameters that influence the geothermal reservoir.

Inversion of MT alone is subject to static shift problems and, therefore, it is recommended that TEM data must be jointly inverted with MT to give a more reliable result, especially in high-temperature volcanic systems.

## ACKNOWLEDGEMENTS

I would like to thank the United Nation University and the government of Iceland for this wonderful opportunity to be one of the 2013 UNU-GTP Fellows. I would also like to extend my appreciation to Mineral Resource Authority for releasing me for this training, particularly Mr. Nathan Mosusu, for his support and encouragement leading up to the training.

My modest and sincere gratitude is extended to my supervisors, Mr. Gylfi Páll Hersir, Mr. Andemariam Teklesenbet and Mr. Knútur Árnason for their excellent help, guidance, advice, tireless work and the knowledge passed during the project season.

My heartfelt thanks are extended to the outgoing Director, Dr. Ingvar Birgir Fridleifsson, and his successor, Mr. Lúdvík S. Georgsson, for their encouraging words and support from start to finish of this training. Special thanks to Ms. Thórhildur Ísberg, Mr. Markús A.G. Wilde, Ms. Málfríður Ómarsdóttir

and Mr. Ingimar G. Haraldsson, for their help in getting things done administratively and for personal matters.

I am also thankful to the class of 2013 UNU-GPT for friendship and help through the highs and lows of life in Iceland.

Lastly, I wish to acknowledge my wife for the commitment and patience during the 6 months of training, and to whom I dedicate this work.

## REFERENCES

Árnason, K., 1989: *Central loop transient electromagnetic sounding over a horizontally layered earth*. Orkustofnun, Reykjavik, report OS-89032/JHD-06, 146, 54-67.

Árnason, K., 2006a: *TEMX (A graphical interactive program for processing central-loop TEM data, short manual)*. ISOR Iceland GeoSurvey, Reykjavik, 10 pp.

Árnason, K., 2006b: *TEMTD (Program for 1D inversion of central-loop TEM and MT data)*. ISOR Iceland GeoSurvey, Reykjavik, short manual, 16 pp.

Árnason, K., Flóvenz, Ó.G., Georgsson, L.S., and Hersir, G.P., 1987a: Resistivity structure of high-temperature geothermal systems in Iceland. *International Union of Geodesy and Geophysics (IUGG) XIX General Assembly, Vancouver Canada, Abstracts V*, 477.

Árnason, K., Haraldsson, G.I., Johnsen, G.V., Thorbergsson, G., Hersir, G.P., Saemundsson, K., Georgsson, L.S., Rögnvaldsson, S.Th., and Snorrason, S.P., 1987b: *Nesjavellir-Ölkelduháls, surface exploration 1986*. Orkustofnun, Reykjavik, report OS-87018/JHD-02 (in Icelandic), 112 pp + maps.

Björnsson, S. (ed.), 1971: Reykjanes, final report on the exploration of the geothermal field. Orkustofnun, report (in Icelandic), 190 pp.

Cagniard, L., 1953: Basic theory of the magneto-telluric method of geophysical prospecting. *Geophysics*, 18, 605-635.

Cantwell, T., 1960: *Detection and analysis of low-frequency magnetotelluric signal*. PhD thesis, M.I.T., Department of Geology and Geophysics, Cambridge, Ma. USA, 171 pp.

Dakhnov, V.N., 1962: Geophysical well logging. *Q. Colorado Sch. Mines*, 57-2, 445 pp.

Einarsson, P., 1991: Earthquakes and present-day tectonism in Iceland. In: Björnsson, S., Gregersen, S., Husebye, E.S., Korhonen, H., and Lund, C.E. (editors), *Imaging and understanding the lithosphere of Scandinavia and Iceland. Tectonophysics*, 189, 261-279.

Flóvenz, Ó.G., Hersir, G.P., Saemundsson, K., Ármannsson, H., and Fridriksson Th., 2012: Geothermal energy exploration techniques. In: Sayigh, A., (ed.), *Comprehensive renewable energy, vol. 7*. Elsevier, Oxford, 51-95.

Franzson, H., Thórdarson, S., Björnsson, G., Gudlaugsson, S.Th., Richter, B., Fridleifsson, G.Ó., and Thórhallsson, S., 2002: Reykjanes high temperature field, SW-Iceland, geology and hydrothermal alteration of well RN-10, *Proceedings of the 27<sup>th</sup> Workshop on Geothermal Reservoir Engineering*, Stanford University, Stanford, Ca, SGP-TR-171, 8 pp.

Fridleifsson, G.Ó., and Albertsson, A., 2000: Deep geothermal drilling at Reykjanes Ridge: Opportunity for an international collaboration. *Proceedings of the World Geothermal Congress 2000, Kyushu-Tohoku, Japan*, 3701-3706.

Georgsson, L.S., 1981: A resistivity survey on the plate boundaries in the western Reykjanes peninsula, Iceland. *Geothermal Resources Council, Trans.*, 5, 75-78.

Georgsson, L.S., 2013: *Geophysical exploration*. UNU-GPT, Iceland, unpublished lecture notes.

Hersir, G.P., 2013: *Resistivity of rocks*. UNU-GTP, Iceland, unpublished lecture notes.

Hersir, G.P., Árnason, K., and Vilhjálmsson, A.M., 2013: 3D inversion of magnetotelluric (MT) resistivity data from Krýsuvík high temperature geothermal area in SW Iceland. *Proceedings of the 38<sup>th</sup> Workshop on Geothermal Reservoir Engineering, Stanford University, Stanford, Ca*, 14 pp.

Jones, A.G., 1988: Static shift of magnetotelluric data and its removal in a sedimentary basin environment. *Geophysics*, 53-7, 967-978.

Keller, G.V., and Frischknecht, F.C., 1966: *Electrical methods in geophysical prospecting*. Pergamon Press Ltd., Oxford, 527 pp.

Pedersen, L.B., and Engels, M., 2005: Routine 2D inversion of magnetotelluric data using the determinant of the impedance tensor. *Geophysics* 70, 33-41.

Phoenix Geophysics, 2009: *User's guide*. Phoenix Ltd., manual.

Quist, A.S., and Marshall, W.L., 1968: Electrical conductances of aqueous sodium chloride solutions from 0 to 800°C and at pressures to 4000 bars. *J. Phys. Chem.*, 72, 684-703.

Rowland, B.F., 2002: *Time-domain electromagnetic exploration*. Northwest Geophysical Associates, Inc., 6 pp.

Scarlato, P., Poe, B.T., Freda, C., and Gaeta, M., 2004: High pressure and high temperature measurements of electrical conductivity of basaltic rock from Mount Etna, Sicily, Italy. *J. Geophys. Res.*, 109-B02210, 11 pp.

Sigurdsson, Ó., 2010: The Reykjanes seawater geothermal system – Its exploration under regulatory constraints. *Proceedings of the World Geothermal Congress 2010, Bali, Indonesia*, 2 pp.

Sternberg, B.K., Washburne, J.C., and Pellerin, L., 1988: Correction for the static shift in magnetotellurics using transient electromagnetic soundings. *Geophysics*, 53, 1459-1468.

Tikhonov, A.N., 1950: Determination of the electrical characteristics of the deeper strata of the earth's crust. *Dokl. Akad. Nauk, USSR*, 73, 295-297 (in Russian).

Ussher, G., Harvey, C., Johnstone, R., and Andersson, E., 2000: Understanding the resistivities observed in geothermal systems. *Proceedings of the World Geothermal Congress 2000, Kyushu-Tohoku, Japan*, 1915-1920.

Verave, R.T., 2013: *Appendices to the report: "Detection and delineation of geothermal resources using 1D joint inversion of MT and TEM data with practical applications from Reykjanes geothermal field, SW-Iceland."*. UNU-GTP, Iceland, report 35 appendices, 71 pp.

Vozoff, K., 1972: The magnetotelluric method in the exploration of sedimentary basins. *Geophysics* 37, 98-141.

Vozoff, K., 1991: The magnetotelluric method. In: Nabighian, M.N (ed.), *Electromagnetic methods. Applied Geophysics*, 2, 641-711.

Ward S.H., and Hohmann G.W., 1987: Electromagnetic theory for geophysical applications In: Nabighian, M.N. (ed.), *Electromagnetic methods in applied geophysics, volume I, theory*. Society of Exploration Geophysicists, Tulsa, OK, 131-311.

Xue, G.Q., Gelius, L.-J., Xiu, L., Qi Z.P., and Chen, W.Y., 2013: 3D pseudo-seismic imaging of transient electromagnetic data – a feasibility study. *Geophysical Prospecting*, 61 (suppl. 1), 561-571.